THE CLOUD DYNAMICS AND RADIATION DATABASE
A FOCUS ON OROGRAPHIC PRECIPITATION

by

Joseph A. Hoch

A thesis submitted in partial fulfillment of

the requirements for the degree of

Master of Science

(Atmospheric and Oceanic Sciences)

at the

UNIVERSITY OF WISCONSIN-MADISON

2006

ABSTRACT

Passive microwave remote sensing of precipitation from platforms such as the Special Sensor Microwave Imager (SSM/I), the Advanced Microwave Scanning Radiometer (AMSR), and the Tropical Rainfall Measurement Mission (TRMM) has been a major focus in hydrological research for the past several years. Estimation of precipitation from these platforms relies on the accuracy of the particular retrieval algorithm being utilized. Retrieval algorithms are based on cloud radiation databases (CRDs) that relate in-situ measurements of brightness temperatures to a-priori microphysical profiles located in CRDs.

A potential problem with a CRD retrieval based approach is that profiles can be chosen that are unrepresentative of the dynamical and thermodynamical state of the atmosphere. Recently, the concept of the Cloud Dynamics and Radiation Database (CDRD) for precipitation retrieval purposes has been introduced. The CDRD is an improved version of current CRDs. The CDRD contains the same information as present CRDs, but in addition contains information about the dynamical and thermodynamical structure of the atmosphere.

The CDRD contains dynamical and thermodynamical tags that are computed from a cloud-resolving model. The cloud resolving model used to build the CDRD is the University of Wisconsin Non-Hydrostatic Modeling System (UW-NMS). These simulations are also used to calculate brightness temperatures and microphysical profiles. During a particular retrieval global forecast models can be used to more accurately mine

the CDRD database, retrieve a more accurate microphysical profile, and thus improve precipitation retrieval.

The main objective of this thesis is to first discuss the methodology for implementing the CDRD system over the entire globe and to show the possibility of retrieving useful subsets of information from a large global database system. The primary technique for extracting useful subsets of information is through the use of data mining techniques. Several data mining techniques are presented and discussed. Orographically enhanced precipitation is fairly challenging to accurately represent from microwave platforms and the current CRD approach. A detailed case study over central and southern California focuses on orographically enhanced precipitation retrieval. The CDRD leads to more accurate microphysical profiles retrieved for the particular event. Finally, Bayes' Theorem, along with the CDRD, is used to more accurately predict the probability of snowfall over the western United States for a particular storm.

The CDRD is a robust system that improves microwave precipitation retrieval techniques. This system can also be used for many other earth science applications. In the future the CDRD will be used to investigate the relationships between microphysical quantities and atmospheric parameters.

ACKNOWLEDGEMENTS

I would like to thank all the people involved in helping me accomplish the maximum amount possible over the past two years. During my time here, I have increased my theoretical knowledge of meteorology and also my love for the weather. First, I would like to thank my advisor, Dr. Greg Tripoli. I have been able to learn a lot from interacting with him over the past two years. He provided just the right amount of guidance for my research, while also letting me working independently. Another benefit of working with Greg was that I could join the AOS bowling team. Whenever the weather was not that exciting, Greg and I could always talk “bowling strategy”.

I would also like to thank my research project colleagues, Dr. Carlo Medaglia, Dr. Amita Mehta, Dr. Alberto Mugnai, and Dr. Eric Smith. It has been a pleasure working with them and I hope to continue collaborations in the future. I am definitely looking forward to visiting Carlo in Rome, Italy.

Thanks also to all my friends I have made over the past two years for all of your support. Anytime work would get a little crazy they were always there to get away from it all. Also, thank you to all the professors I have had the opportunity to interact with over the past two years, there are far too many to list by name.

My choice to attend the University of Wisconsin turned out to be a great decision. I will never forget the football games, the tornado chasing, the hurricane chasing, the skiing, and the opportunity to grow as a scholar in the field of meteorology.

TABLE OF CONTENTS

CHAPTER 1: INTRODUCTION

Passive microwave remote sensing of precipitation from space is a relatively new concept in the field of meteorology. Not until the late 1970's and early 1980's were the first attempts made to accurately retrieve rainfall estimates from space. Two of the earliest microwave platforms were Nimbus-6 and Nimbus-7. After the launch of these satellites, research in precipitation retrieval from space flourished (Wilheit 1976, Liou 1979, Prabhakara 1986, Wilke 1986, Spencer 1987, Petty 1990, 1992). Since the Nimbus program many other microwave satellite platforms have been launched, including the Scanning Multichannel Microwave Radiometer [*SMMR*, *1981- 1987*] (Prabhakara 1986), the Special Sensor Microwave/Imager [*SSM/I*, *1987 – present*] (Ferriday 1994), the Advanced Microwave Scanning Radiometer [*AMSR*, *2002 – present*] (McCollum 2005), and the Tropical Rainfall Measurement Mission Microwave Imager [*TRMM*, *1997 – present*] (Kummerow et al. 1998). Improvement of passive microwave remote sensing of precipitation is still a key scientific goal. A new National Aeronautics Space Agency (NASA) mission is currently planned that will further enhance the capabilities of precipitation remote sensing (i.e. the Global Precipitation Measurement Mission [*GPM*]).

Current microwave remote sensing platforms return radiance measurements over an observational satellite footprint. These radiance measurements can be converted to corresponding brightness temperatures. The most common range for microwave frequencies on these platforms is from 10 GHz through 89 GHz. In current retrieval schemes, brightness temperatures are matched to corresponding precipitation rates with similar microphysical precipitation structure. Precipitation retrieval schemes require Cloud Resolving Model (CRM) simulations of several different types of precipitation systems, precipitation structure, and the microphysical properties of the simulated environment. One of the most commonly used microwave precipitation retrieval algorithms is the Goddard Profiling Algorithm [*GPROF*] (Kummerow 2001).

Retrieval schemes make use of a-priori databases that relate microwave frequency brightness temperatures to surface precipitation rates through simulated microphysical specifications (hydrometeor sizes, shapes, and distributions). These databases are produced from CRM simulations. GPROF utilizes a cloud radiation database (CRD) that was produced from the Goddard Cumulus Ensemble Model (GCE) and the University of Wisconsin Non-Hydrostatic Modeling System (UW-NMS). The CRD contains vertical estimates of the simulated microphysical structure of the atmosphere, commonly referred to as "*microphysical profiles*". Estimates of the six categories of hydrometeors (i.e. rain, snow, pristine ice, graupel, aggregates, and cloud) are contained within each profile.

Although shown to be fairly accurate, passive microwave remote sensing retrieval schemes could be improved. Often various configurations of hydrometeors can produce similar brightness temperatures. Thus, microphysical properties taken from the a-priori CRD can be mixed from differing atmospheric environments. Orographic precipitation is one particularly challenging area for current retrieval schemes. This problem could be caused by the CRD database consisting of mainly tropical simulations (Kummerow 2001). The small scale variability and shallow precipitation structure could also cause some of the biggest retrieval errors. Satellites often look straight through the shallow liquid water path of orographic storms.

The overall goal of this research is to develop a new retrieval scheme to improve the accuracy of matching observed brightness temperatures and a-priori microphysical precipitation structure. The Cloud Dynamics and Radiation Database (CDRD) is the proposed improvement on the current CRD approach. The CDRD includes all of the typical information of a CRD, but also simulated dynamical and thermodynamical tags. At the time of retrieval, microphysical profiles can be selected from both observed satellite measurements and dynamical/ thermodynamical tags to estimate surface precipitation rates. By using a tag-based retrieval approach, constrained by a Bayesian algorithm, there is potential to reduce the variability of retrieved microphysical profiles, thus improving precipitation retrieval.

Improving satellite precipitation retrieval is essential for accurate measurement and understanding of the global water cycle. More accurate retrieval can also be used for data assimilation purposes and better model forecasts. The proposed CDRD techniques improve the accuracy and usefulness of retrieval from current satellite platforms.

This thesis is organized as follows. Chapter 2 discusses currently available passive microwave remote sensing platforms. These instruments include SSM/I, AMSR, and TRMM. The upcoming Global Precipitation Measurement mission is also discussed. An overview of GPROF is presented, along with the necessity for the CDRD approach.

Chapter 3 explains the CDRD concept in more detail. Microphysical profile, dynamic tag, and thermodynamic tag variables are presented. Database tags are selected based on their ability to distinguish differing atmospheric environments. The associated CRM nested 3-grid setup is discussed.

Chapter 4 describes the predictive models used to formulate the CDRD system. These models include the University of Wisconsin Non-Hydrostatic Modeling System and the Successive Order of Interaction (SOI) radiative transfer model. The setup for these models is discussed, along with various other details. Also, Bayes' theorem is presented as a useful technique to search through the CDRD database system.

Chapter 5 focuses on the theory of orographically enhanced precipitation. As mentioned, orographic precipitation is a challenging quantity to accurately diagnose from satellite measurements. Past research and orographic field studies are presented to determine appropriate CDRD tags to correctly diagnose orographically enhanced precipitation.

Chapter 6 presents an orographic precipitation case study. The UW-NMS is used to simulate a severe orographic event that occurred from January 7^{th} – 11^{th}, 2005 over the Sierra Nevada region of California. The case study includes several sensitivity tests, along with examples of data input into the CDRD.

Retrieval of CDRD profiles is accomplished through data mining techniques. Data mining is a powerful tool used to search through large database systems, commonly referred to as the data warehouse. Chapter 7 presents commonly used mining techniques and the current CDRD approach. Data mining is one of the main highlights of the CDRD retrieval approach because of its effectiveness and efficiency.

Chapter 8 presents an overview of potential CDRD applications. A simulated retrieval of microphysical profiles over the California case study region is discussed. Using the CDRD approach reduces the amount of variance in retrieved microphysical profiles, thus leading to more accurate profiles. Also, a global application using the CDRD for snowfall probability retrieval is discussed. Through the use of CDRD tags and Bayes' Theorem, the level of certainty in precipitation retrieval can be increased. Finally, conclusions and future work are discussed.

CHAPTER 2: PRECIPITAITON RETRIEVAL ALGORITHMS

Currently passive microwave remote sensing platforms, available for precipitation retrieval, are AMSR, SSM/I, and TRMM. In upcoming years, a follow-up mission to TRMM will be launched, the Global Precipitation Measurement mission. Potential problems with the retrieval algorithms and the need for a CDRD approach are discussed.

a. Microwave Satellite Platforms

The Special Sensor Microwave/Imager, launched in 1987, provides an opportunity to study over 15 years of data. There have been six different SSM/I platforms, all carefully inter-calibrated. The SSM/I is part of the Defense Meteorological Satellite Program (DMSP) satellite program. Data from the SSM/I is often used to calculate ocean wind speeds, water vapor fields, cloud water fields, and surface rain rates. The SSM/I is part of the NASA Pathfinder program. The resolution of the 85.5 GHz channel is 12.5km. The satellites are in sun-synchronous, circular, and nearly polar orbits. The swath width is approximately 1400km, with global coverage.

The Advanced Microwave Scanning Radiometer was launched on May 4th, 2002, on the NASA's Aqua spacecraft. Over the oceans, AMSR can measure several different parameters such as sea surface temperatures (SST), wind speeds, water vapor, cloud water, and rain rates. Mean spatial resolutions decrease with increasing center frequencies from 56km to 5.4km for the 89.0 GHz channel. This represents a significant increase in resolution from the 12.5km resolution of the SSM/I. The satellite footprint of

AMSR for the 89.0 GHz channel is 6 x 4 km. This is a large increase compared to the 15 x 13km footprint for SSM/I.

The Tropical Rainfall Measurement Mission was launched in November 1997. The purpose of this mission was to map precipitation variability over the entire tropical belt. The TRMM not only contains a microwave imager, but also an onboard radiometer. The TRMM Microwave Imager (TMI) is very similar to the SSM/I radiometer. The TMI measures the intensity of radiation at five separate frequencies, 10.7, 19.4, 21.3, 37, and 85.5 GHz, dual polarization. These frequencies are similar to those of the SSM/I, except that TMI has the additional 10.7 GHz channel designed to provide a more-linear response towards high rainfall rates. Another improvement of TMI is the increased resolution. This is mainly a function of a lower orbit altitude. TMI has a 487 mile (780-kilometer) wide swath on the surface. The higher resolution of TMI, as well as the additional 10.7 GHz frequency, makes TMI a better instrument than its predecessors.

The TRMM K_U Precipitation Radar (PR) measures reflectivity over a narrow swath. Reflectivity measurements can be used to infer rain rates via a Z-R relationship. The PR direct precipitation measurements are then used to calibrate the wide measurement swath of the TMI.

TRMM has been a vital mission used to produce frequency distributions of rainfall intensity and coverage, partition stratiform and convective precipitation events, measure the vertical distribution of hydrometeors, and make tropical measurements of latent heat release. TRMM has also aided in the study of atmospheric teleconnections, such as the Madden-Julian oscillation, the Asian monsoon, and ENSO events.

TRMM has provided invaluable data over the tropical regions of the globe. The need now exists to study precipitation outside of the tropical regions. To accomplish this goal, NASA is planning the next generation satellite mission, the Global Precipitation Measurement mission.

The Global Precipitation Measurement mission (GPM) will continue the work of TRMM. This satellite is an improved version of TRMM, including increased spatial resolution and increased coverage area. One of the biggest improvements is the addition of dual-frequency precipitation radar (DPR). The DPR will have a 5km resolution at 13.6 GHz K_U band and 35.5 GHz K_A band. The GPM radars will have the ability to measure, via reflectivity and estimates of attenuation, the vertical profiles of clouds and precipitation, including the drop size distribution. The GPM Microwave Imager (GMI) will have a swath width of 850km. It contains the same frequencies as TRMM at higher spatial resolutions and four additional high frequency millimeter-wave channels at about 166 GHz and 183 GHz. The current scheduled launch date of GPM is 2012.

Space-borne microwave technology has significantly improved from SSM/I through TRMM. Resolutions and spatial coverage have both increased. Table 1 shows a summary of the available microwave frequencies on these instruments. These frequencies are used by precipitation algorithms to estimate surface precipitation rates. In formulating the CDRD system these channels are all considered, with the majority included.

SSM/I	AMSR	TRMM	GPM
19.4 V&H	6.925 V&H	10.7 V&H	10.7 V&H
22.2 V&H	10.65 V&H	19.4 V&H	19.0 V&H
37.0 V&H	18.7 V&H	21.3 H	22.0 V&H
85.5 V&H	23.8 V&H	37.0 V&H	37.0 V&H
	36.5 V&H	85.5 V&H	85.0 V&H
	50.3 V		150 V&H
	89.0 V&H		183.3 V&H

Table 1. Available microwave frequencies on current satellites.

b. The Goddard Profiling Algorithm (GPROF)

The GPROF rain rate algorithm uses statistical inversion techniques, based upon theoretically calculated relations between rainfall rates and brightness temperatures. Inverse hydrometeor profiles are used to explicitly account for the potential errors introduced in the GPROF theoretical calculations. This is accomplished by allowing various vertical distributions in the theoretical brightness temperature calculations and by requiring consistency between the observed and calculated brightness temperatures (Kummerow and Giglio 1994). Smith et al. (1998) states that the cloud model generated profiles in the GPROF algorithm are assigned a-priori probabilities. These are related to brightness temperatures at all SSM/I frequencies and polarizations through a forward RTE model. The GPROF rain rate algorithm explicitly accounts for the vertical structure of precipitation within a cloud. This vertical structure is a key factor in determining the upwelling radiances. The algorithm simulates the upwelling radiances by means of a radiative transfer scheme (Kummerow and Giglio 1994).

Different configurations of hydrometeors can produce similar brightness temperatures. Thus, a potential problem with the CRD retrieval is that particular profiles, featuring the best match to observed brightness temperatures, can be taken from differing atmospheric conditions. Microphysical profiles could be combined from stratiform and convective events, cold frontal and tropical systems, unstable and stable atmospheres, or other potential situations. If inaccurate matching occurs, the microphysical profile produced from the CRD weighting functions would be an inaccurate representation of the true microphysical structure of the atmosphere, which leads to errors in the rainfall estimation.

The proposed solution is to develop an improved version of current CRDs. The CDRD, discussed in more detail in the next chapter, includes all the typical information of a CRD, but also dynamical and thermodynamical tags paired with each microphysical profile. At the time of retrieval, profiles are obtained not only from satellite brightness temperatures but also a wide variety of tags. These tags should reduce the amount of unrepresentative environmental profiles selected.

CHAPTER 3: CLOUD DYNAMICS AND RADIATION DATABASE (CDRD)

An operational global database has been implemented using daily randomly selected simulations beginning on August 1st, 2005. A global database, including randomly selected simulations, is necessary for several reasons. First, it is important to obtain a robust database warehouse with many possible meteorological conditions. In order to utilize this system for global precipitation retrieval, all meteorological events such as stratiform, convective, tropical, frontal, cellular, orographic, etc. must be represented in the CDRD. Second, using daily simulations captures seasonal variations. Finally, random CRM simulations, using the UW-NMS, are important to eliminate any biases towards particular precipitation events or geographic regions.

A two-way nested grid structure is used with three grids for CDRD simulations. The innermost domain size of these simulations is approximately 5 degrees by 5 degrees. The resolutions of these grids are 50km, 10km, and 2km respectively. When a CRM simulation begins, a 12Z Global Forecasting System (GFS), 9-hour model precipitation prediction is used to sample the selected random innermost domain. This prediction is necessary to test if the selected location has the potential to produce precipitation in the mesoscale simulation. This GFS test is mainly used because of computational resources. Current mesoscale simulations take approximately 24 hours to produce a 12 hour forecast. If a region shows no sign of precipitation in the GFS forecast a new random location is selected.

The UW-NMS performs a 12 hour simulation over the selected location. Microphysical profiles, dynamical, and thermodynamical tags for the CDRD database are saved at the 12 hour simulation time. Information is stored in the database only for the

12-hour forecast time to allow for spin-up and local forcing to develop. Often it takes 12 hours for accurate tropical cyclone spin-up. Microphysical profiles are saved based on simulated surface precipitation rates. The criteria for saving a profile is taken to be when surface rain rates are 0.50 mm hr^{-1} or greater and/or a frozen (snow, graupel, aggregates, pristine crystals) surface precipitation rates are 0.25 mm hr^{-1} or greater. These criteria are selected based on the capability of current microwave remote precipitation sensors. These precipitation criteria are near the accepted lower limits of useful satellite data (Wilheit 2003). The following table shows the variables that make up a microphysical profile. The corresponding data is saved at all 36 vertical model levels at each appropriate grid point. As discussed earlier, these microphysical profiles are necessary to convert radiance measurements to precipitation estimates.

Hydrometeor Measurements (Rain, Snow, Graupel, Aggregate, Pristine Crystals)	**Other Profile Variables**	
Mixing Ratio (g/kg)	Total Condensate Mixing Ratio (g/kg)	Pressure (hPa)
Concentration (#/cm^3)	Water Vapor Mixing Ratio (g/kg)	Height (m)
Diameters (micrometer)	Cloud Water Mixing Ratio (g/kg)	Temperature (K)
Terminal Velocity (cm/s)	Surface Skin Temperature (K)	Zonal Wind (m/s)
Densities (g/cm^3)	Latent Heating Term (K/day)	Meridional Wind (m/s)
Surface Rate (mm/hr)	Diabatic Moisture Term (K/day)	Vertical Velocity (m/s)
		Liquid Coating Flag

Table 2. UW-NMS variables included in a standard "microphysical profile".

Dynamical and thermodynamical tags are paired with microphysical profiles at two different resolutions, 50km grid spacing (low resolution) and 2km grid spacing (high resolution). The majority of variables are saved at low resolution so that they are comparable to global model resolutions, such as the Global Forecasting System (GFS). New precipitation retrievals will use microwave brightness temperatures paired with the following CDRD dynamical tags, obtainable from global operational models, which are shown in the next two tables. These tags should provide for more accurate microphysical profiles selected from the CRM database, thus improving precipitation estimation. The selection of CDRD profiles is based on a Bayesian approach. Bayesian techniques, discussed further in a later chapter, use the dynamical tags to more accurately sample available profiles.

50KM GRID SPACING TAGS

Mean Sea Level Pressure (hPa)	Freezing Level (m)	Surface Theta Gradient (K/m)	LFC Height (m)
Surface Temperature (F)	Lifted Index (K)	700mb Theta Gradient (K/m)	LCL Height (m)
**U-Wind (m/s)	Froude Number	Surface Theta-E Gradient (K/m)	Topography Height (m)
**V-Wind (m/s)	Surface Theta-E (K)	700mb Theta-E Gradient (K/m)	PBL Height (m)
U Momentum Flux (kg/ms^2)	Surface Brunt Vaisala Frequency (s^{-1})	** Q Vector Convergence	Richardson Number in the PBL
V Momentum Flux (kg/ms^2)	**Temperature (K)	Surface Divergence (s^{-1})	Potential Vorticity Advection at 700 and 250 mb ($Kkgm^3/s^2$)
CIN (J/kg)	Potential Vorticity at 700 and 200 mb (PVU)	Divergence at 700 and 200 mb (s^{-1})	Height of Maximum CAPE (m)
Maximum CAPE (J/kg)	Surface Vertical Vorticity (s^{-1})	**Vertical Velocity (m/s)	Diabatic Moisture Term (K/day)
Surface CAPE (J/kg)	Vertical Vorticity at 700 and 200 mb (s^{-1})	Theta-E minimum (K)	Latent Heat Term (K/day)
Kinetic Energy (J)	0-6km Wind Shear (s^{-1})	500 and 850 mb thickness (m)	**Specific Humidity (g/kg)

Table 3. Large Scale (50km) Dynamic/Thermodynamic Tags included in the CDRD.v1 system.
** Represents vectors (1000, 925,850,700,500,250,200,150,100 mb)

5KM GRID SPACING TAGS

Cloud Ceiling (m)	** Temperature (K)
Topography Height (m)	** Q Vector Convergence (m^2/skg)
Largest Topography Neighbor Difference (m)	** Vertical Velocity (m/s)
Direction of Topography Direction (degrees)	Cloud Fraction
PBL Height (m)	Convective Cloud Fraction
Mean Sea Level Pressure (hPA)	Stratiform Cloud Fraction
Surface Pressure (hPA)	

Table 4. Small Scale (5km) Dynamic/Thermodynamic Tags included in the CDRD.v1 system. ** Represents vectors (1000, 925,850,700,500,250,200,150,100 mb)

The dynamical/ thermodynamical tags were selected based on their ability to differentiate between particular atmospheric environments. For example, consider the following meteorological events and the appropriate CDRD tags:

- **Convective vs. Stratiform Precipitation –** *Vertical Velocity, Cloud Fraction, Wind Shear, CAPE*
- **Tropical or Non-Tropical Environment –** *MSLP, Temperature, Theta-E, Freezing Level, Thickness, Latitude*
- **Severe Weather Environment –** *CAPE, CIN, Lifted Index, Theta-E, Vertical Velocity, Wind Shear, Divergence*
- **Inertial Gravity Wave Environment –** *Momentum Flux, Temperature, Froude Number, Brunt-Vaisala Frequency*
- **Mid-latitude Storm –** *MSLP, Temperature, Specific Humidity, Winds, Potential Vorticity, Vertical Velocity, Thickness*

- **Orographic Influence –** *Topography Height, Topography Slope, Winds, Momentum Flux*
- **QG-Forced Motion –** *Q-Vector Convergence, Divergence, Potential Vorticity Advection, Temperature*

Microwave frequencies included in the database are 6.6 GHz, 10.65 GHz, 18.7 GHz, 19.35 GHz, 23.8 GHz, 36.5 GHz, 85.5 GHz, 89.0 GHz, 150 GHz, and 183.3 GHz. All of these channels are dual polarization, vertical and horizontal, except 23.8 GHz. These channels were selected based on present and future satellite platforms, as discussed in the previous chapter.

CHAPTER 4: CDRD MODELING SYSTEMS

The following section outlines three different types of models used in the CDRD design. The first model discussed is a mathematical model, Bayes' theorem. This mathematical model is the basis for future CDRD precipitation retrieval algorithms. GPROF also uses Bayesian statistical techniques to obtain the best estimated microphysical profiles. The other two models are atmospheric models, the UW-NMS and the SOI radiative transfer model.

a. Bayes' Theory

The CDRD is designed to support a Bayesian framework for precipitation retrieval. A Bayesian approach is similar to a statistical inversion algorithm that achieves a maximum likelihood estimate, while being trained by the CDRD. Bayes' theorem is used to obtain certain optimal parameters, such as microphysical profiles, from a set of measurements, i.e. the dynamical tags.

Bayes' theorem, for the purpose of rain rate retrievals, can be expressed as the following:

$$P(R \mid Tb) = P(R) \times P(Tb \mid R)$$

Equation 1. Bayes' Theorem expressed in terms of rain rate (R) and brightness temperatures (TB).

Vertical distributions of hydrometeor profiles are expressed by **R** and vertical distribution of brightness temperatures are expressed by **Tb**. The goal of the CDRD retrieval scheme is to find a particular hydrometeor profile given a certain brightness temperature, P(R|Tb). The probability that a certain hydrometeor profile will be observed, P(R), is produced from the mesoscale model. The second term on the right side of the equation, P(Tb|R) is produced from radiative transfer schemes. The benefits of a Bayesian based approach are shown in a later chapter with an operational CDRD retrieval.

b. University of Wisconsin Non-Hydrostatic Modeling System

The UW-NMS is used to create mesoscale simulations for the CDRD input. The model is described in full detail by Tripoli (1992). One of the most fundamental reasons for using the UW-NMS is its unique terrain following system, variable step topography. The following figure is an example of this terrain system.

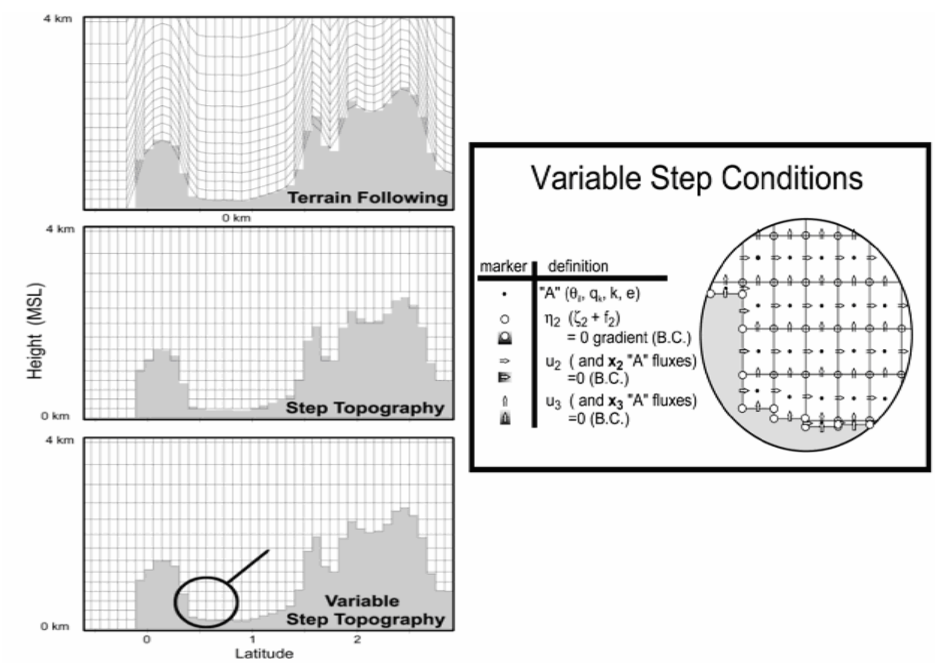

Figure 1. Three different mesoscale modeling terrain systems.
The UW-NMS uses a unique Variable Step Condition to specify terrain.

Other mesoscale models represent terrain in various ways such as terrain following systems or step topography systems. Terrain following systems do not accurately resolve very steep topography, as shown in figure 1. Step topography systems have difficulty resolving subtle changes in topography, as shown in the same figure. The UW-NMS terrain following system is capable of handling both these scenarios very well. Since the UW-NMS invokes such an advanced terrain system, it is capable of reproducing various terrain induced flows. Tripoli shows many classic terrain problems modeled accurately by the UW-NMS (1992). In a later chapter the UW-NMS is used to study an orographically enhanced precipitation event over California.

The UW-NMS uses a two-way nesting scheme. The largest grid is usually taken to be hydrostatic, unless non-hydrostatic information exists. The outer grid initial data may be interpolated from another model run such as the NCEP or European Center for Medium range Weather Forecast (ECMWF) models, or may be initialized from a horizontally homogeneous state, such as a sounding (Tripoli 1992). All CDRD simulations are initialized from Global Forecasting System (GFS) analysis files. The large-scale dynamic tags are taken from the outer grid while the high resolution tags are from the inner grid domain.

c. Successive Order of Interaction (SOI) Radiative Transfer Model

The amount of time required running model simulations globally and building a complete database requires a fast, yet fairly accurate, radiative transfer code for the purposes of this project. The Successive Order of Interaction (SOI) Radiative Transfer Model, developed by Ralf Bennartz at the University of Wisconsin, is utilized for computation of microwave brightness temperatures. This model computes a brightness temperature field for a given frequency and polarization in about two minutes.

The SOI is a 1-dimensional azimuthally-averaged, plane-parallel radiative transfer model. This model includes the effects of scattering from all hydrometeors. The SOI ignores atmospheric polarization, but not surface polarization (Heidinger et al. 2004). This is a hybrid model which uses both the doubling method and the Neumann method, which involves successive order of scattering, to obtain the upwelling radiance. The figure below illustrates the structure of the SOI model. Notice the doubling and successive order scattering properties of the model.

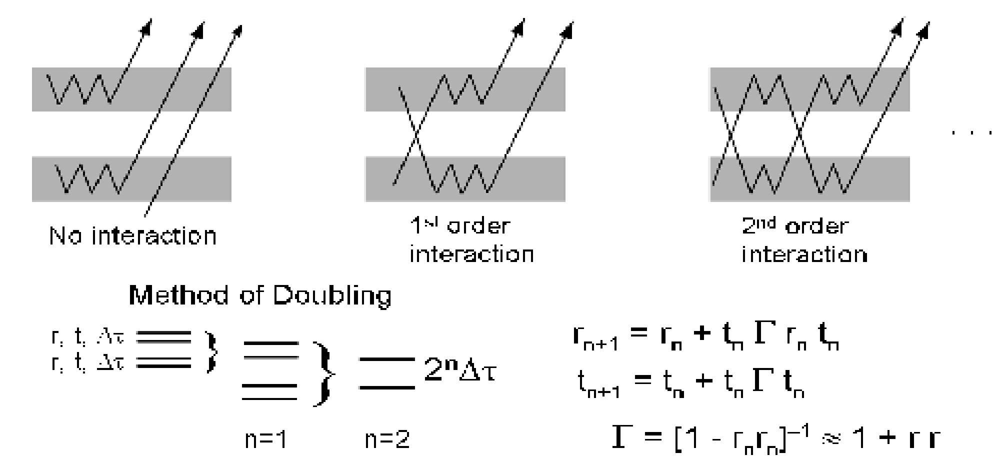

Figure 2. Doubling method used in the Successive Order of Interaction (SOI) radiative transfer model.

CHAPTER 5: OROGRAPHIC PRECIPITATION

Orographic precipitation is the cause of many extreme flooding events over mountainous regions worldwide and a challenge to accurately measure from space-based instruments. This chapter highlights the mechanisms of orographic precipitation formation and the potential dynamic and thermodynamic tags that should be included in the CDRD system. Some previous orographic field experiments are discussed to determine the appropriate CDRD tags for detection of this type of precipitation. In this section the CDRD tags are highlighted in bold. CDRD tags can be used to diagnose all the known types of orographic precipitation. These tags, along with satellite measurements, can identify previously undetectable precipitation.

Seven mechanisms for the production of orographic precipitation, documented by Houze (1993), are now discussed. Figure 3 is an example of these seven different orographic precipitation mechanisms.

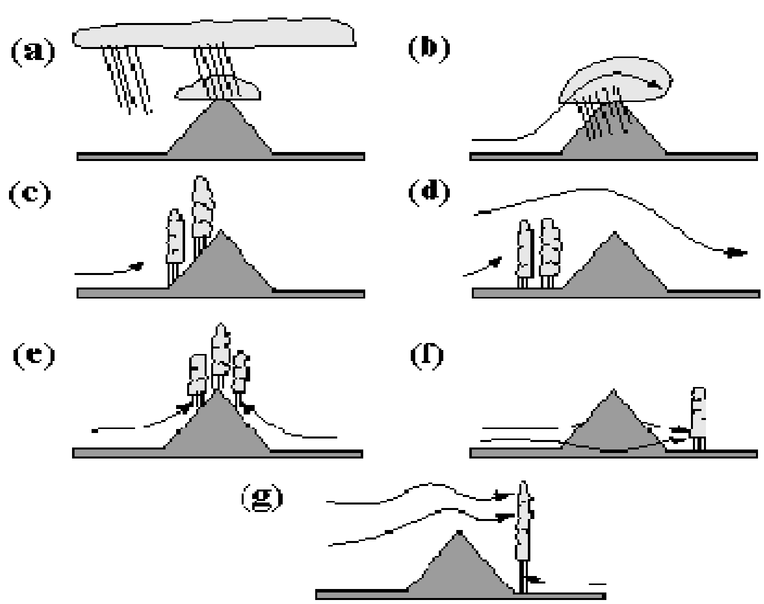

Figure 3. Seven possible mechanisms leading to the formation of orographic precipitation.

The first mechanism is the "Seeder-Feeder". During this processes ice crystals, from a glaciated stratiform cloud aloft, fall onto a cloud of supercooled droplets, which were initially generated by the orography. The glaciation process is referred to as the "Bergeron-Findeisen process". Water droplets are most prevalent (at temperatures warmer than about -20^{o}C) but ice crystals are more efficient centers of growth from the vapor stage. This follows from the difference between the values of saturation vapor pressure over an ice surface when compared with a water surface. In "mixed" clouds, containing both liquid and ice, the air is close to being saturated with respect to liquid water, but is super-saturated (an unstable phase) with respect to ice. Consequently, in mixed clouds, ice crystals grow from the vapor phase much more rapidly than do the nearby droplets. This growth method, first documented by Bergeron (1935), is the Bergeron - Findeisen process. **Vertical temperature structure** is a key variable to recognize this process and is included in the CDRD.

The second orographic mechanism involves the presence of stably stratified air. This air can be forced to rise over the mountain range. As the air rises, it cools, becomes saturated, and precipitation can result. This is one of the most common types of orographic rainfall, especially in the mid-latitudes (Houze 1993). The condition of whether a given air parcel will go over a mountain is given by the Froude number (Fr), as shown in equation 3.

$$Fr = \frac{U}{h_m N}$$

U = Wind Speed
h_m = Mountain Height
N = Brunt-Väisälä frequency

Equation 2. Froude Number calculation.

In most simple terms, the Froude number can be thought of as a ratio of kinetic energy to potential energy. If the Froude number is greater than 1 the air parcel will make it over the mountain, if it is less than 1 then it will not, and if it is equal to 1 then the air parcel reaches the mountain top with zero velocity. For low Froude number flows (less than 1) this simple physical reasoning suggests that the flow is essentially blocked by the topography and must either go around or be turned back. For this precipitation formation mechanism it is assumed that the Froude number is greater than one. The **Froude number** and **topography height** are included in the CDRD to diagnose this type of orographic influence.

The third mechanism to form orographic precipitation involves a potentially unstable atmosphere. For potential instability theta-e must decrease with height, as shown in equation 4.

$$\frac{d\theta_e}{dz} < 0$$

Equation 3. Criteria that defines a potential unstable atmosphere.

The mountain acts as a trigger to the convection. As air is forced to rise in this unstable environment, deep convection can occur. Often thunderstorms are found between the foothills and the crest of the mountain range. **Theta-E** and **Theta-E gradients** are included in the CDRD system.

The fourth precipitation formation mechanism involves the creation of a surface boundary, such as in temperature, dew point, and/or wind. The mountain can create a pseudo dryline effect and trigger deep convection downstream. A sharp gradient in temperature or dew point can cause a gradient of mass from each air mass. The lighter air mass is forced to rise over the more dense air. This rising air often then triggers convection. A gradient in wind speeds may produce enough shear to supplement long lived thunderstorms. **Temperature**, **dew point**, **wind**, and **wind shear** are all dynamic variables included in the CDRD.

The fifth mechanism is very similar to the fourth described above. In the presence of calm large-scale winds, especially at low levels, the mountain may induce boundary-layer flows. These flows develop due to the difference in daytime heating and nighttime cooling. Convergence of these flows may trigger thunderstorm formation. Houze (1993) notes that this is the leading mechanism for orographic precipitation enhancement near the Inter-Tropical Convergence Zone (ITCZ).

The final two mechanisms, leeside convection enhancement and convection triggering, are often overlooked mechanisms for the formation of orographic rainfall. These mechanisms are especially prevalent near an isolated mountain peak. If air is stable and can not be forced over the mountain, which implies the Froude number is less than one, it must go around the mountain. As air is forced around the mountain leeside convergence may result in updrafts and/or rainfall enhancement. Convection can be triggered due to this convergence. Again, this mechanism highlights the importance of including the **Froude number** in the CDRD.

These seven mechanisms are thought to be responsible for the formation of orographic precipitation. In the following case study the second orographic precipitation mechanism is responsible for enhancement of precipitation.

a. Previous field studies

With a process as complex as orographic precipitation, the best way to gain understanding of the phenomenon is to take real-time measurements and analyze the data collected. Numerous field programs have focused on trying to better understand the process of orographic precipitation. Three such field programs are now discussed in more detail to understand which dynamical tags should be included in the CDRD.

The Mesoscale Alpine Programme Intensive Observing Period 2B (MAP IOP-2B) took place from September 18^{th} - 21^{st}, 1999, the Intermountain Precipitation Experiment (IPEX) took place from January 31^{st} - February 25^{th}, 2000, and the California Landfalling Jets Experiment (CALJET) took place during the winter of 1997/98.

A heavy precipitation event, forced by orography, occurred on September 19^{th} and 20^{th}, 1999 which was observed and later modeled by Lin et al. (2004). This event occurred over the Alps, near the Lago Maggiore region, during the MAP IOP-2B period. The Pennsylvania State University/ National Center for Atmospheric Research Mesoscale Modeling system (PSU/NCAR MM5) is used as a modeling tool for this event. During this event, a deep trough helped to evaporate moisture from the Adriatic Sea and advect moisture into the Alps region. One of the key results from this study is the importance of a strong impinging low level jet (LLJ), coupled with the influx of a moisture source. Lin et al. (2004) showed that the low-level convergence created by the mountain barrier creates a convergence zone which helps increase precipitation amounts.

Shafer et al. (2005) looked at the influence terrain has on synoptic and mesoscale precipitation distributions during IPEX. One of the goals of this field experiment was to advance the understanding about orographically enhanced precipitation, with a focus on the Wasatch Mountains of Utah. This field experiment focused on data-assimilation for the purpose of improving mesoscale model predictions of quantitative precipitation forecasts over complex terrain.

Shafer et al. (2005) studied an occluded front approaching the Sierra Nevada mountain range. In this study the occluded front could not surmount the mountain range, while the upper-level trough moved over the mountain region unimpeded. This resulted in a discontinuous low-level storm evolution. This study is important because it shows that the low-level structure of a midlatitude cyclone can be strongly influenced by terrain, while upper-level features move relatively unimpeded by the terrain.

The final field project and most applicable to this research is the California Landfalling Jets Experiment, which occurred during the winter of 1997-98. Neiman et al. (2002) studies the relationship between upslope flow and rainfall in the California coastal mountain region. Neiman et al. (2002) looks at individual cases, low-level jet cases and the entire winter season. Linear correlations between average upslope flow components versus rain rate are as high as 0.94 for individual storm cases. The low-level jet cases are around 0.75 and the entire winter season is around 0.75 (Neiman et al. 2002). This research study shows that the layer of flow that best influences orographic precipitation is near the mountain, around 1 km above sea level for the California coast. Neiman et al.

(2002) discusses that orographic precipitation is also controlled by ambient thermodynamic stratification and dynamic flow around topography, availability of moisture, precipitation formation efficiency, and latent heat release. On the simplest level, orographic precipitation is controlled by the upslope flow influence (Neiman et al. 2002).

From these field experiments variables such as available **moisture**, **low-level winds**, **vertical pressure distribution**, **terrain slope**, **theta-e**, and **latent heat release** are shown to be important for detecting various types of orographic precipitation. All of these variables are included in the CDRD system. The following chapter shows the ability of the UW-NMS to predict orographic events and an application of the CDRD for a simulated orographic event.

CHAPTER 6: CASE STUDY - CALIFORNIA OROGRAPHIC STORM

The period of January 7th through January 11th, 2005 brought tremendous amounts of rainfall and snowfall throughout much of California. Areas such as Nordhoff Ridge and Opids Camp recorded over 25 inches of equivalent rainfall during the event. The storm caused millions of dollars in damage and at least 10 deaths due to mudslides. This storm was particularly damaging for the region as a similar storm system had just impacted the area from December 26th through January 5th, 2005.

The main branch of the jet stream brought a low-pressure system off the coast of British Columbia. A relatively strong subtropical jet stream provided the necessary moisture over the entire region. The high-pressure system further west in the Pacific Ocean set up a blocking pattern that kept the jet stream in the relatively same position for several days. Another low-pressure system became stationary off the coast of California, helping to further stream subtropical moisture into the region. During the four day period the precipitable water reached values as high as 1.5 inches. As impulses moved onto the California coast winds flowing counterclockwise intersected the Sierra Nevada mountain chain and caused heavy orographic precipitation enhancement.

As is the case with many storms in California, the mountainous terrain of the region enhanced the precipitation. Previous studies have commonly focused on the Sierra Nevada region because of the regular occurrence of this type of precipitation enhancement (Marwitz 1987; Reynolds and Kuciauskas 1988; Colle 2004; Dettinger et al. 2004; Galewsky and Sobel 2005). The following case study is used to highlight the application of the CDRD system and the ability of the UW-NMS mesoscale model to simulate orographic precipitation.

The UW-NMS is used to simulate the four-day event. A three grid nesting system is used with an outer grid resolution of 50km, middle grid resolution of 10km, and an inner grid resolution of 2km. The largest time step on the outermost grid is 90 seconds, 22.5 seconds on the middle grid nest, and 11.25 seconds on the innermost grid. The UW-NMS is particularly good at simulating orographically enhanced precipitation due to its variable step topography system.

First, the upper-level dynamics of the storm are analyzed. The focus is on the polar and subtropical jet streams and their impacts during the event. Second, the mid-level dynamics are analyzed using potential vorticity as a diagnostic tool for approaching short waves. Finally, the low-level dynamics are analyzed using 1-km wind flow and surface moisture over the region. All of these variables are included as CDRD tags.

Sensitivity experiments are used to diagnose the amount of orographic influence during the event. It is necessary to determine the sensitivity of the parameters in question to determine if they should be included in the CDRD.

a. Upper-Levels – The Jet Stream

The jet stream plays an important role in most large scale synoptic weather patterns. Jet streams exist due to the baroclinicity of the atmosphere, such as the temperature gradient between the equator and North Pole. An examination of the thermal wind equation, shown in the following equation, can explain the existence of such a feature.

$$f\mathbf{v}_T = \mathbf{k} \times \nabla(\phi_1 - \phi_0)$$

Equation 4. Thermal wind equation.

V_T – Thermal Wind
f – Coriolis Parameter
ϕ – Geopotential Height

The thermal wind circles areas of cold air, for example the North Pole. Thus, in the northern hemisphere winds are westerly. The thermal wind equation shows that these westerly winds will increase with height, thus the existence of the jet stream. This region of fast moving winds is found usually around 12 – 13km.

The most common jet stream is the polar jet. However, a second jet can exist due to the advection of momentum from the equator northwards. This jet stream is commonly referred to as the sub-tropical jet stream. The sub-tropical jet stream is usually found at latitudes of 30 to 40 degrees in general westerly flow, and is important for the transport of moisture.

Jet streams are important for several reasons. First, they influence the direction of synoptic scale features. Second, they can create regions of upper level divergence and convergence. Thirdly, they can influence moisture transport. Finally, they can influence stability and be responsible for gravity wave formation.

Both the polar and sub-tropical jet streams play an important role in the California orographic storm development. Shown in figure 4 is the 3-dimensional wind speed field, as predicted by the UW-NMS. The daily progression of the two jet streams, beginning on January 7^{th} at 12Z through January 11^{th} at 12Z, can be seen. Also shown in figure 4 is a schematic of the large-scale synoptic setup for this event. This image is courtesy of the California Nevada River Forecast Center. The UW-NMS simulation is consistent with this depiction.

The polar jet stream digs a deep trough off the Pacific coast. The jet stream is rather strong from the 7^{th} until the 10^{th} with wind speeds in excess of 75 m/s. The polar jet stream begins to weaken and move northward by the 10^{th} and 11^{th}, as shown in figure 4. The jet stream was basically stationary for 4 straight days continuously steering synoptic disturbances towards the California coast.

As mentioned previously, the sub-tropical jet is also important in this case. The steady sub-tropical jet increases the moisture transport from the equator towards the California coast. As shown in figure 4, the sub-tropical jet stream is rather strong as well nearing values of 60 m/s. Typically, the sub-tropical jet is much weaker than the polar jet. During this event the two jet streams seem to couple, especially on January 8^{th} and 9^{th}. This coupling leads to enhanced jet stream dynamics over the region. During the same two days large-scale gravity waves, caused by the jet stream interaction with the Sierra Nevada and Rocky mountain chains, seem to be evident.

Finally, the associated upper-level divergence caused by the jet stream is an important consideration in this case. Figure 4 shows the favored regions of upper-level divergence caused by the sub-tropical jet. This region is commonly referred to as the “left exit region”. Upper level divergence can lead to enhanced vertical motion due to the conservation of mass.

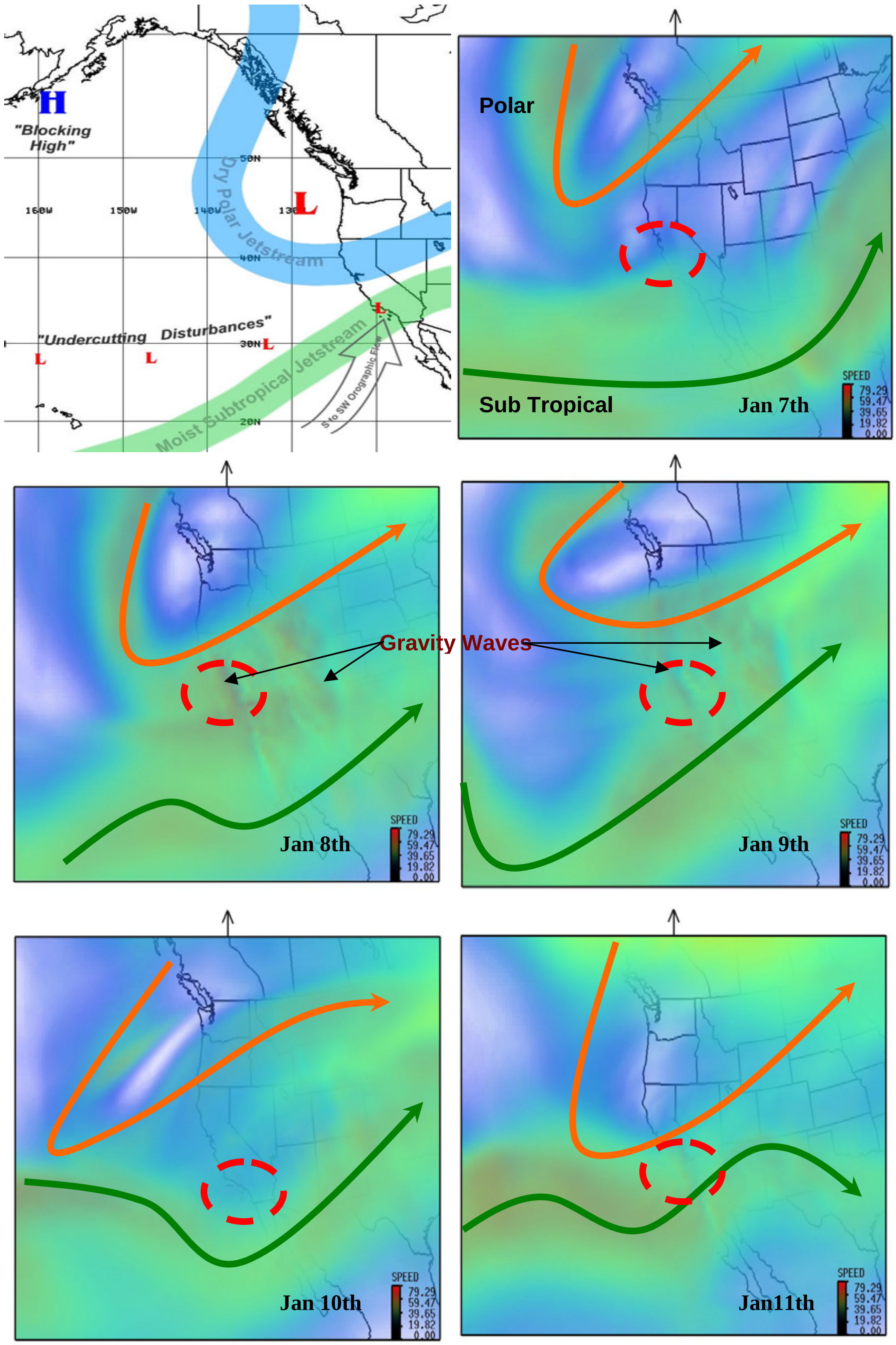

Figure 4. Daily progression of the polar and sub-tropical jet streams from January 7th - 11th at 12Z respectively, as simulated by the UW-NMS.
Upper Left – Synoptic setup for this orographic storm event.

b. Mid-Levels – Large Scale Potential Vorticity

As was shown in the synoptic schematic in figure 4, there were many "undercutting disturbances" steered by the jet streams aloft that enhanced the precipitation over the California coast. One of the best tools to diagnose these disturbances or short waves is to analyze the potential vorticity field. Potential vorticity is a very useful quantity mainly because it is conserved on isentropic surfaces. The following equation is the mathematical definition of isentropic potential vorticity.

$$P = -g(\zeta_\theta + f)\frac{\partial\theta}{\partial p}$$

Equation 5. Mathematical definition of potential vorticity.

P – Isen. PV
g – Gravity
ζ_Θ – Relative Vorticity
f – Coriolis Parameter
$d\theta / dp$ – Diff. change of Theta with Pressure

Since the focus of this section is the mid-level dynamics, 700mb potential vorticity is used as a diagnostic tool. At this level various short waves should be evident.

Shown in figure 5 is the 700mb potential vorticity, as simulated by the UW-NMS, beginning on January 7th at 12Z through January 11th at 12Z. Very evident is the large trough off the Pacific Northwest. High potential vorticity is associated with this trough due to the enhanced cyclonic flow, potentially showing the presence of a tropopause fold. The focus of this section is the various short waves outside the main cyclonic flow. On January 8th, 9th, and 10th these short waves are evident by an increase of PV. It is evident that these waves continuously propagate towards the coast during this time.

Also shown in figure 5 is the 700mb streamline flow. This is useful for qualitatively diagnosing regions of potential vorticity advection. From quasi-geostrophic theory, regions of positive vorticity advection are favored areas for rising motion. This rising motion, along with orographic uplift, helped to enhance precipitation amounts over the California region.

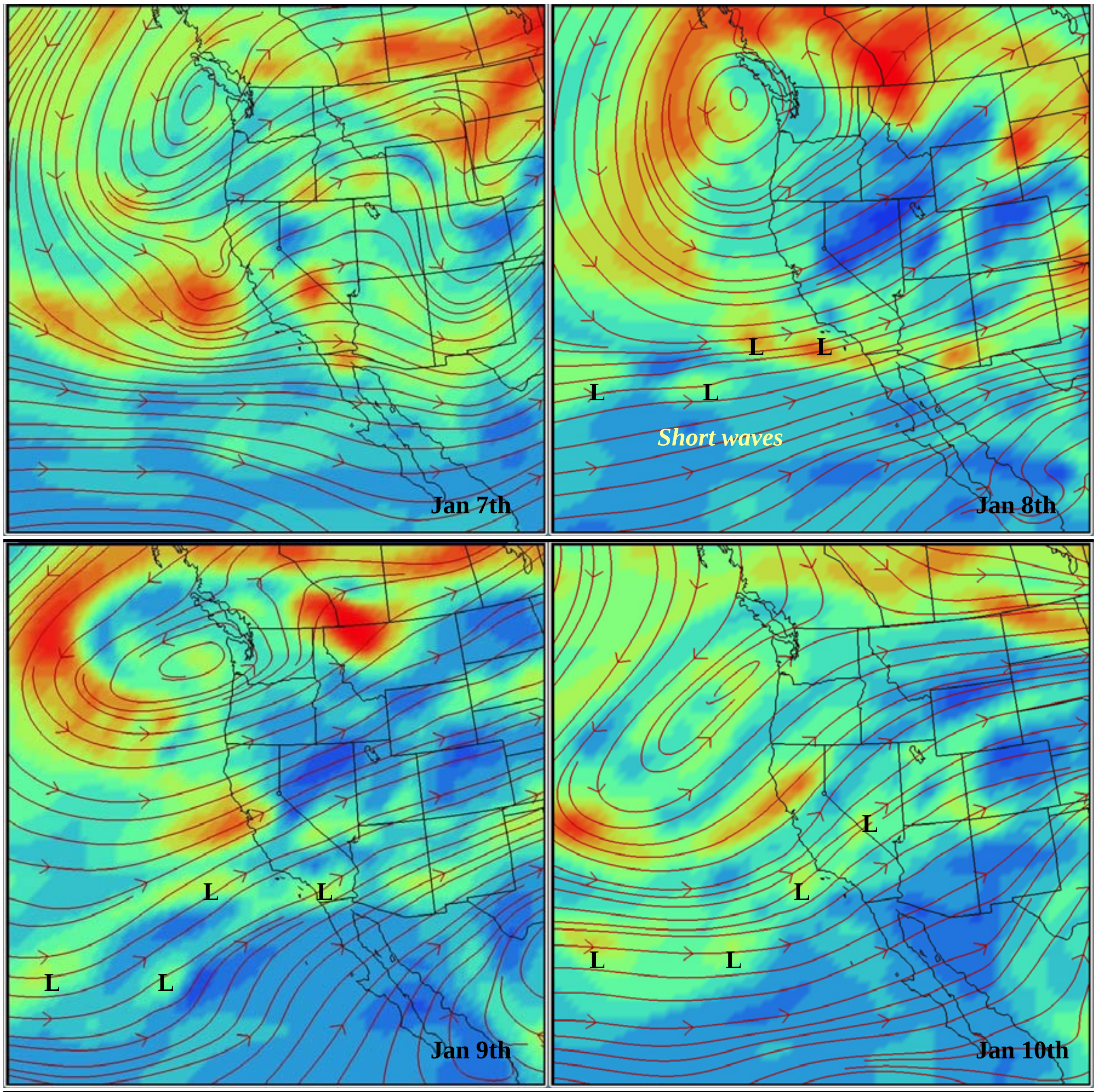

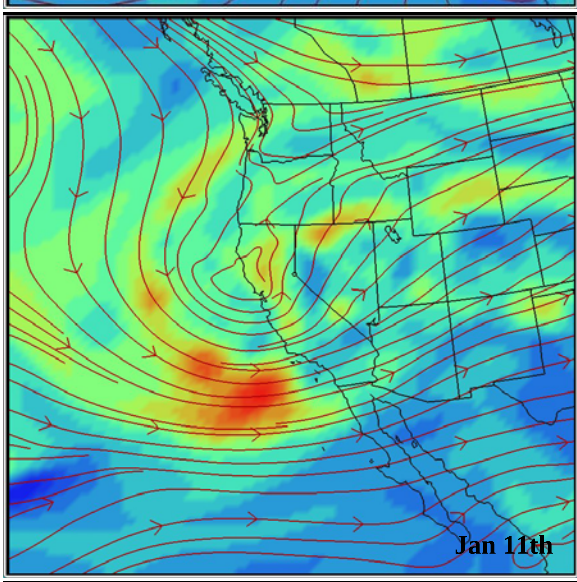

Figure 5. Daily progression of the 700mb Potential Vorticity and 700mb streamlines from January 7th -11th at 12Z respectively, as simulated by the UW-NMS.

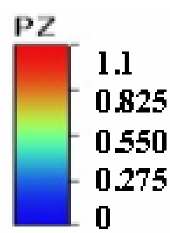

Units - PVU

c. Low-Levels – Moisture and 1km Winds

As discussed in chapter 5, there are many possible mechanisms that can cause the orographic enhancement of precipitation. Although synoptic features such as the jet stream and vorticity are important, arguably two of the most important parameters to diagnose the potential for orographic precipitation are surface moisture and the 1-km wind field. As discussed earlier, the 1-km level is the optimal level for orographic flow in regions where the flow is perpendicular to the mountain chain.

Surface moisture during this event was particularly high. Moisture was lifted over the Sierra Nevada mountain chain orographically and condensed. Water vapor mixing ratio values are often used to diagnose surface moisture content. First, mean values of water vapor mixing ratio over the region of interest must be considered. Shi and Bates (2005) used the High Resolution Infrared Radiation Sounder (HIRS) to produce an eighteen year mean (1979 – 1996) of water vapor mixing ratio. Figure 6 shows this mean water vapor over the continental United States.

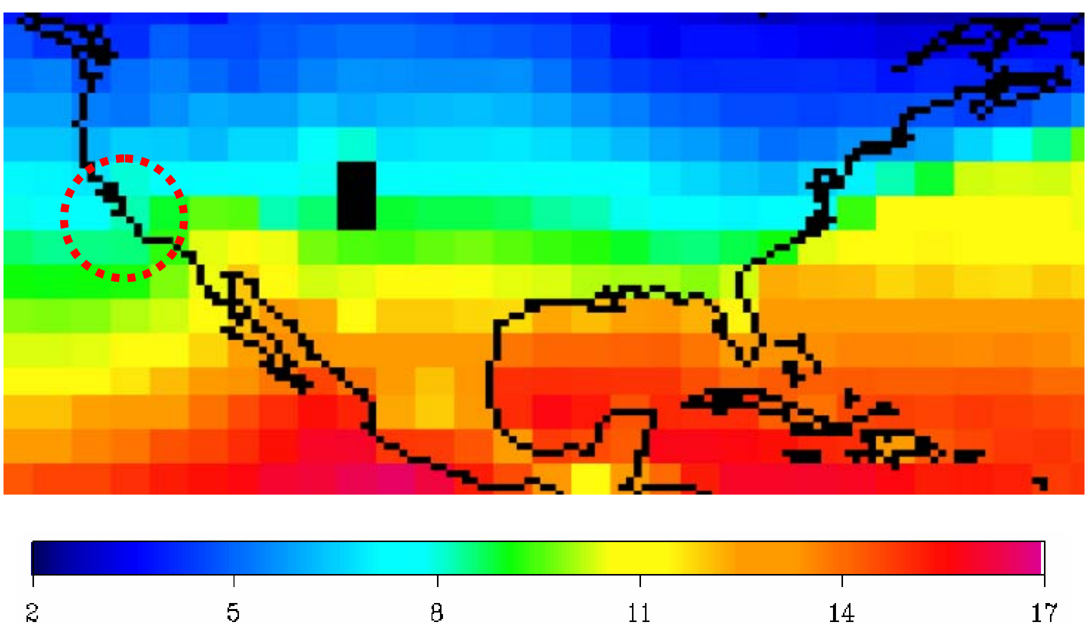

Figure 6. Eighteen-year mean distribution of water vapor mixing ratio at 1005 hPa.

For our region of interest, the annual mean water vapor mixing ratio is approximately 8 g/kg.

Figure 7 shows the daily progression of water vapor mixing ratio and 1-km winds from January 7^{th} – 11^{th} at 12Z, as simulated by the UW-NMS. The dashed circles represent the three main mountain ranges of interest, the San Bernardino Mountains, the Santa Monica Mountains, and the Sierra Nevada Mountains.

First, it is important to consider the position of the wind vectors. During the entire period the 1-km winds are almost perpendicular to the mountain ranges. This provides the optimal conditions for upslope flow. Second, water vapor mixing ratios are high, nearing 10 g/kg throughout most of the period. This highly saturated air is being advected from the Pacific Ocean towards the mountain ranges. It is important to remember that since this event occurred during the winter season when surface temperatures are at their coolest and moisture is lessened. Figure 6 is an annual mean, most likely influenced heavily by the summer months. This illustrates just how high the moisture content for this event was compared to normal.

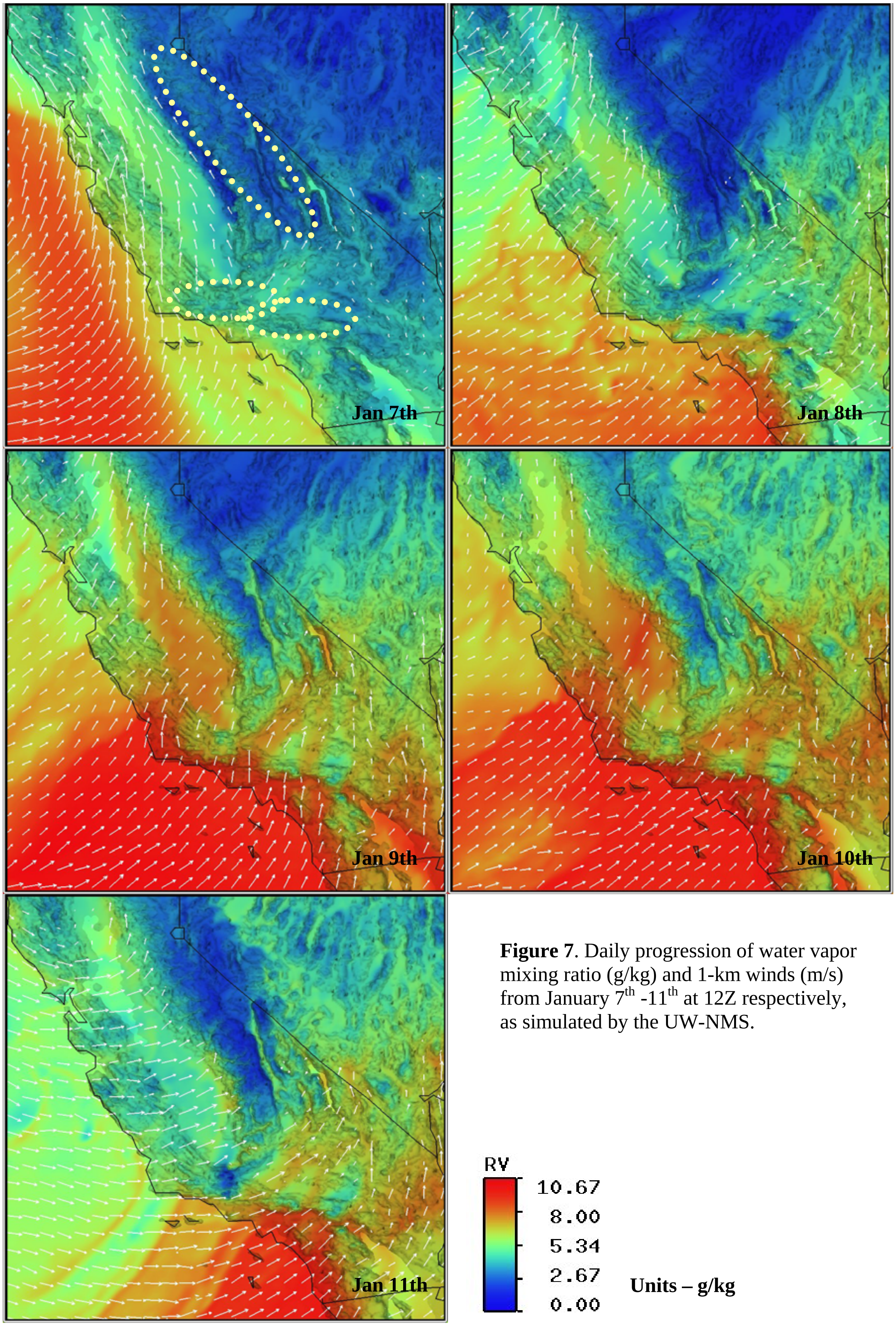

Figure 7. Daily progression of water vapor mixing ratio (g/kg) and 1-km winds (m/s) from January 7th -11th at 12Z respectively, as simulated by the UW-NMS.

d. Precipitation Verification

To verify the accuracy of the simulations, stage IV radar/gauge data is used from the National Centers for Environmental Prediction (NCEP). This data is available over the CONUS at 4km resolution. Stage IV data is a mosaic of regional multi-sensor analysis produced by NWS River Forecast Centers (RFCs). Figure 8 shows the comparison for accumulated precipitation during the four-day period, January 7^{th} – 11^{th}. The first four plots are daily accumulated precipitation amounts, followed by the storm total precipitation amounts. These plots show that the UW-NMS is very successful in precipitation prediction for this synoptic/mesoscale event.

Figure 8 also shows that precipitation was heaviest during the 24-hour period from January 9^{th} to January 10^{th}. Overall the UW-NMS produces realistic results for the daily and total events. As expected, precipitation amounts for the San Bernardino Mountains and the Santa Monica Mountains are highest. These mountains are closest to the moisture source, the Pacific Ocean, as shown in figure 7. Also, 1-km winds flow in the optimal orographic precipitation direction for almost five straight days over these ranges.

One weakness in the simulation was over the San Monica Mountains. Over this region the UW-NMS under-predicts the total precipitation amount. One possible cause is that this mountain range is composed of many isolated peaks. The model may not produce the amount of upslope needed to produce the precipitation, due to the ability to resolve topographic features. Another cause may be from enhancement of precipitation due to an effect from nearby Los Angeles, possibly acting as a heat island. Finally, the lower resolution of the NCEP data may affect the measured precipitation amounts.

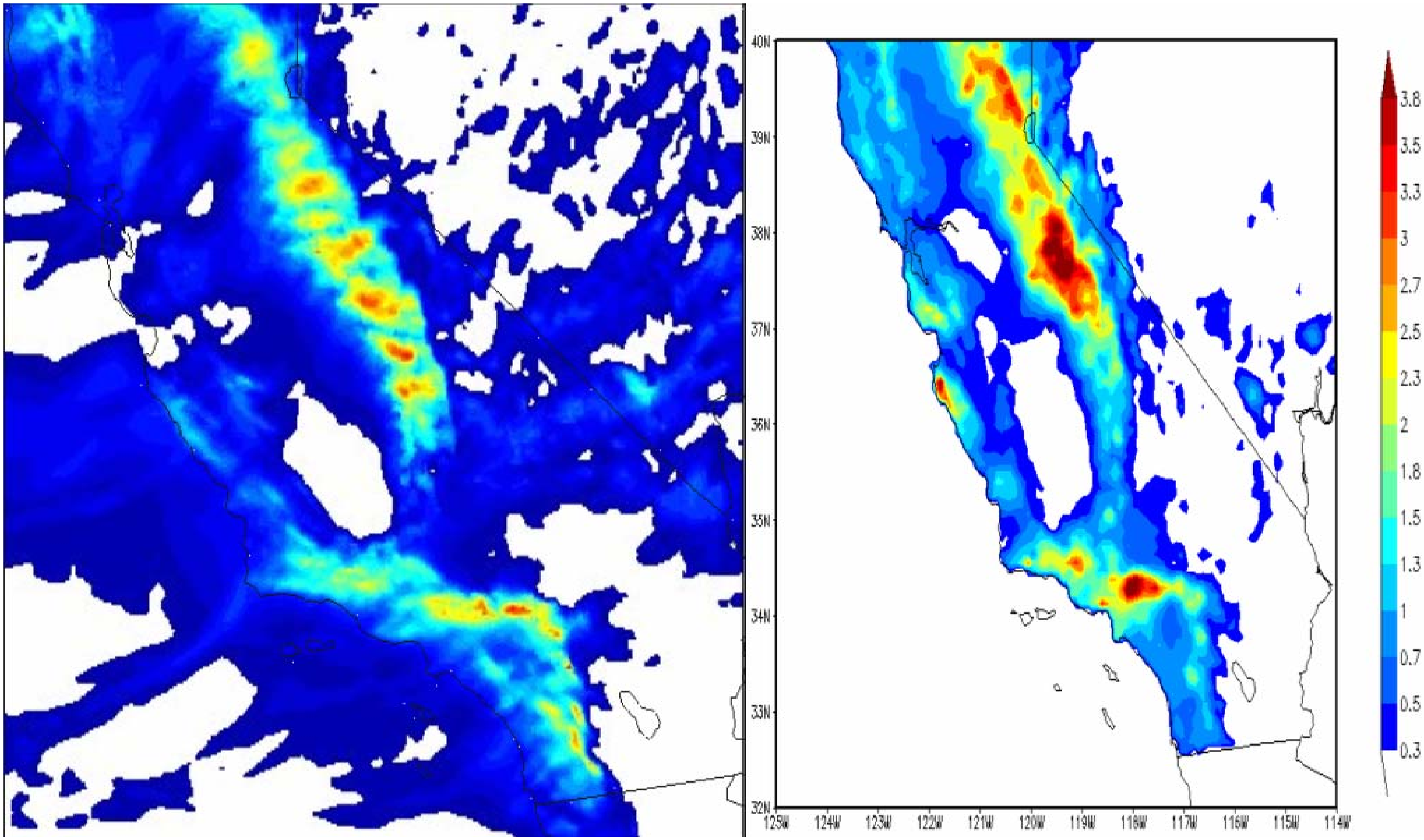

Figure 8a. Accumulated Precipitation from January 7th, 12Z – January 8th, 12Z (in.)
Left – UW-NMS prediction Right – NCEP Stage IV data

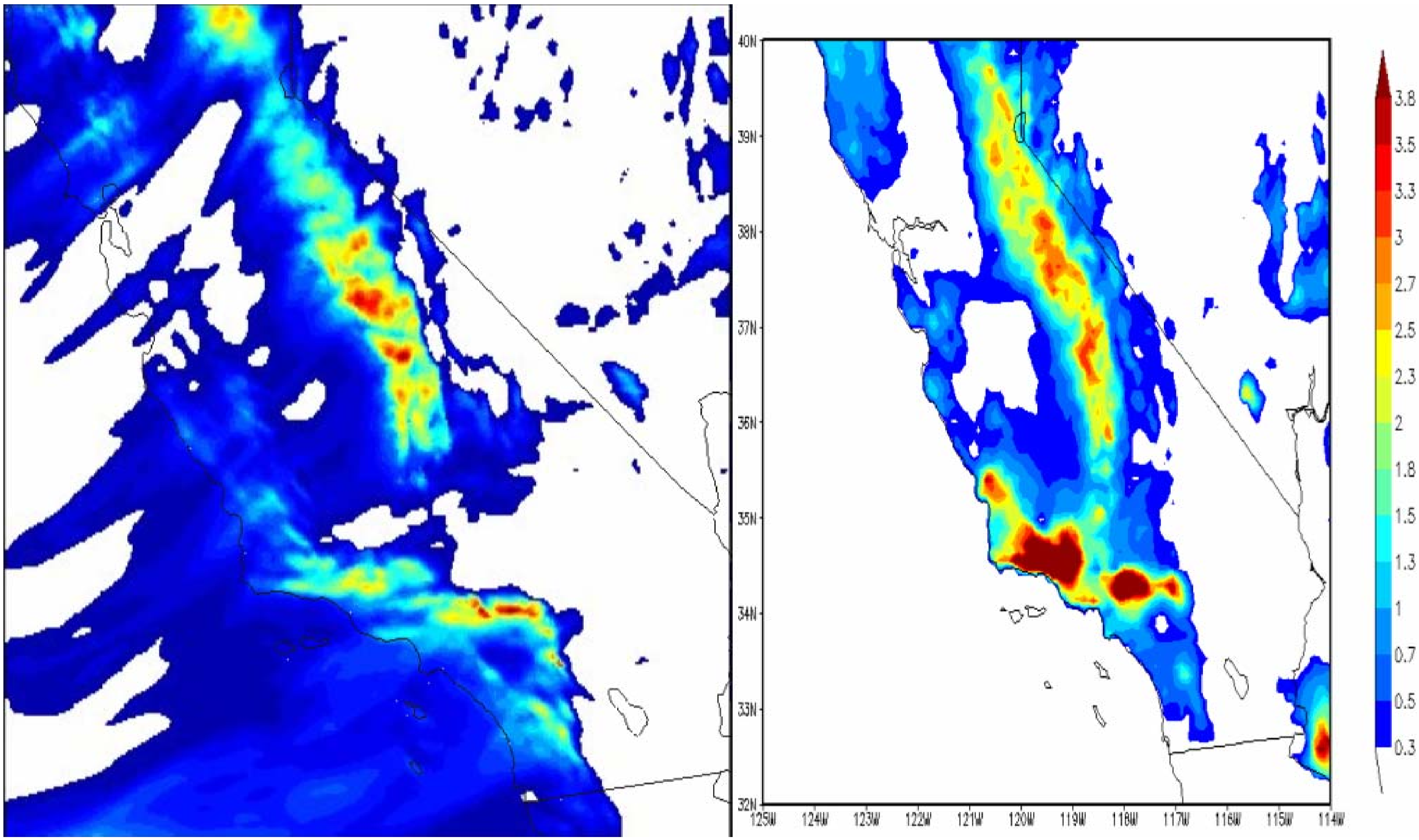

Figure 8b. Accumulated Precipitation from January 8th, 12Z – January 9th, 12Z (in.)
Left – UW-NMS prediction Right – NCEP Stage IV data

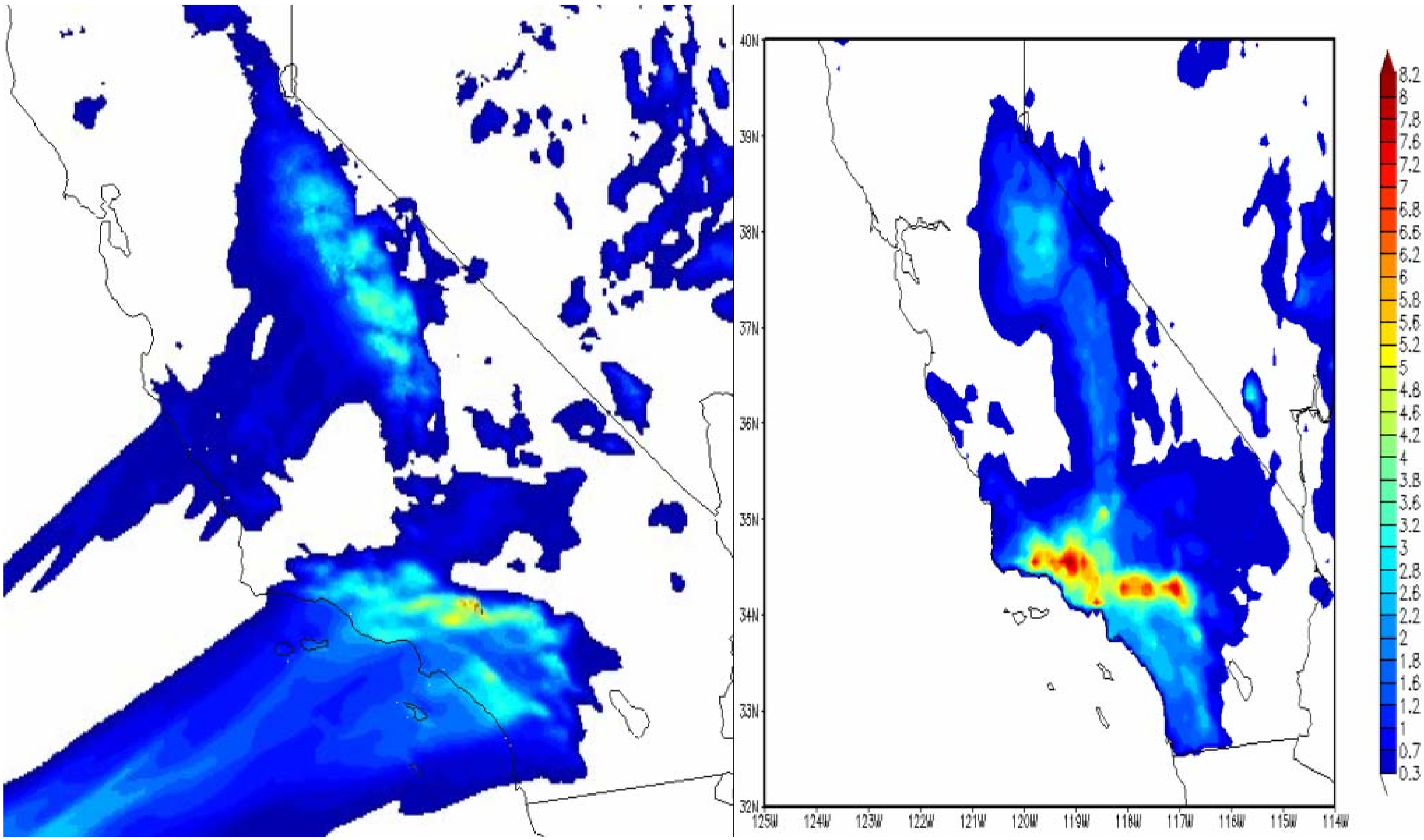

Figure 8c. Accumulated Precipitation from January 9th, 12Z – January 10th, 12Z (in.)
Left – UW-NMS prediction Right – NCEP Stage IV data

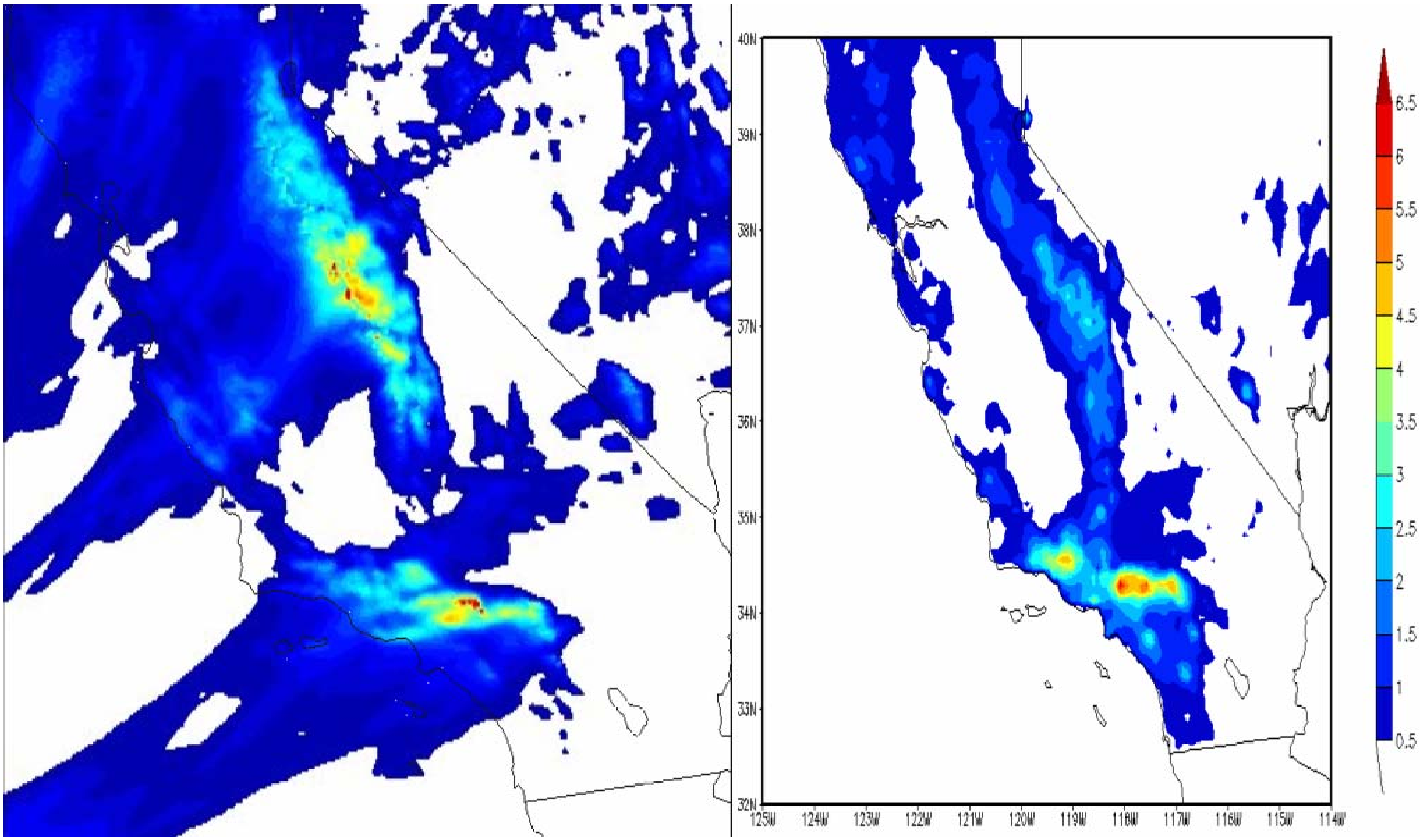

Figure 8d. Accumulated Precipitation from January 10th, 12Z – January 11th, 12Z (in.)
Left – UW-NMS prediction Right – NCEP Stage IV data

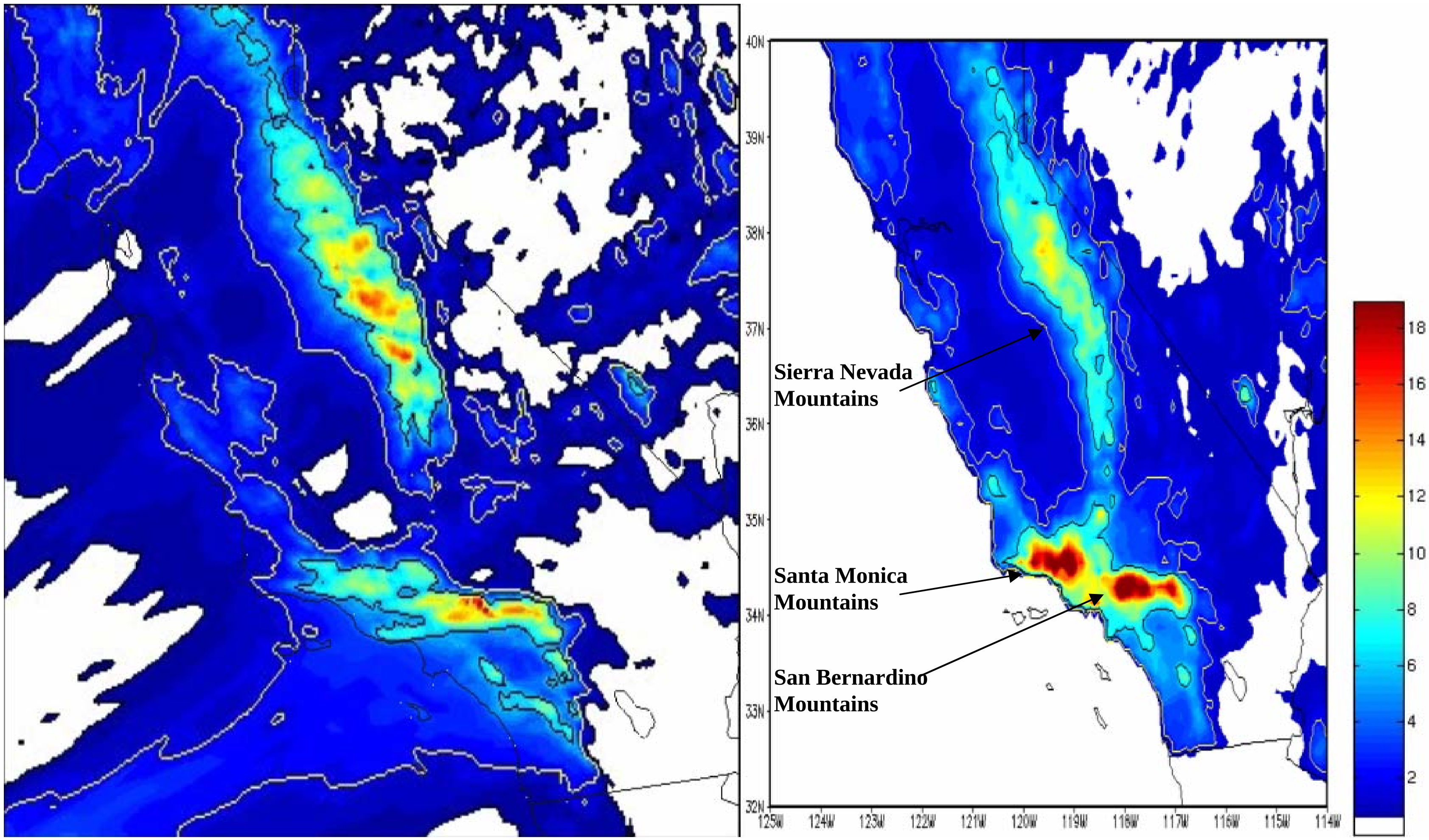

Figure 8e. Accumulated Precipitation from January 7th, 12Z – January 11th, 12Z (in.)
Left – UW-NMS prediction Right – NCEP Stage IV data
Yellow Contour – 4 inches, Black Contour – 7 inches

e. Sensitivity Experiments

One advantage of using models for meteorological events is the opportunity to conduct sensitivity experiments. First, to qualitatively estimate how much precipitation is being influenced by the topography of the region, the same simulation of the California event is run with a flat elevation (no mountain effects). Figure 9 shows the difference in UW-NMS predicted precipitation amounts for the no mountain run minus the control run. Values less than -2 inches are overlaid onto a topography map of California. As expected, the largest differences in precipitation exist directly over the mountain ranges, highlighting the orographic nature of the precipitation. Without the influence of topography precipitation amounts decrease nearly 80 – 90 percent.

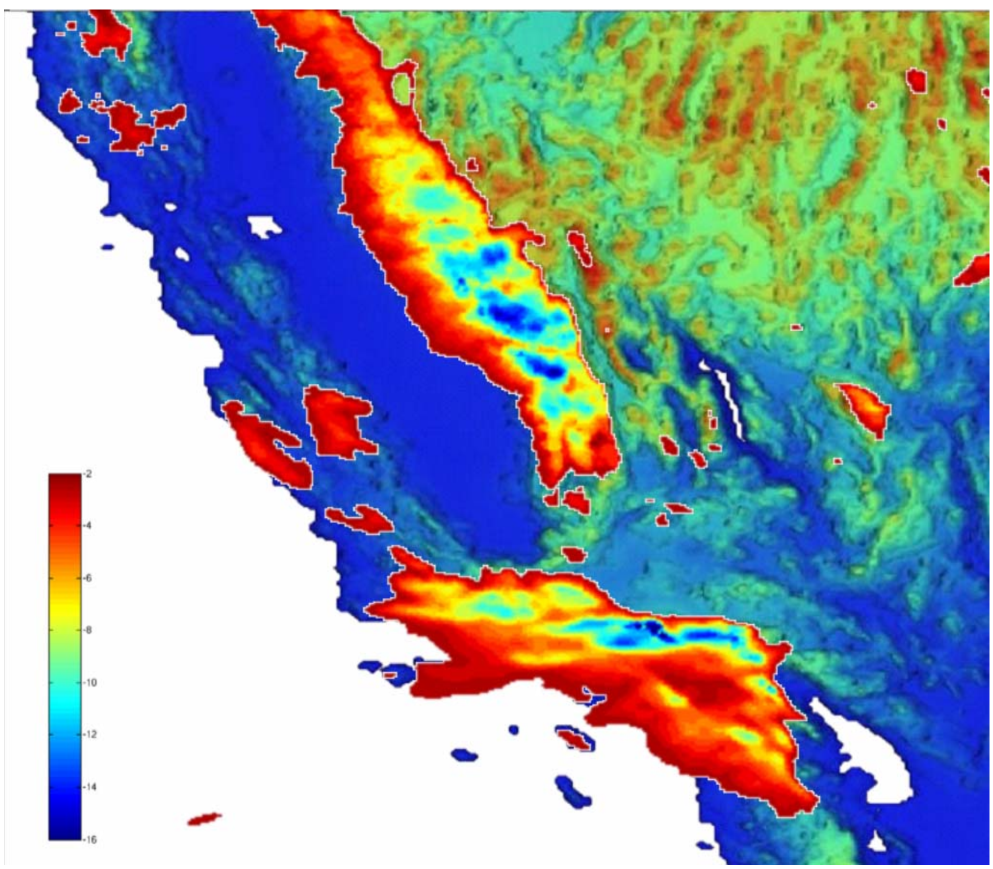

Figure 9. No Mountain precipitation minus Control Run precipitation (inches).

In this case precipitation amounts are directly related to the height and slope of the topography. These two variables are included in the CDRD database as potential retrieval tags.

Since brightness temperatures are essential for precipitation retrieval, it is useful to understand how sensitive these channel temperatures are compared to certain variables. Four variables of particular interest are selected: **elevation**, **slope**, **sea surface temperature**, and **resolution**. New simulations are run for all of the following cases: (a) elevation is increased/decreased 500 meters throughout the inner domain, (b) the topography slope of the Sierra Nevada chain is increased gradually by raising topography by multiples of 30 meters, starting at the bases of the mountain range (increased 30 m) and ending at the apex (increased 600 m), (c) sea surface temperatures are increased/decreased 5 degrees Kelvin, and (d) the resolution of the innermost grid is increased to 1.6 km and decreased to 6.6 km.

Figure 10 shows the change in brightness temperatures for each different adjusted simulation. In each case the new simulation brightness temperature fields are subtracted from the control run brightness temperatures. All of the UW-NMS grids are based on a 252 x 252 grid domain. The scatter plots show the difference in the 89.0 GHz brightness temperatures at each point.

As expected, all investigated parameters show the capability to change the brightness temperatures by a significant amount (20K +). For some parameters, such as the increased sea surface temperature simulation, the brightness temperatures fluctuate by over 100K at some points on the grid.

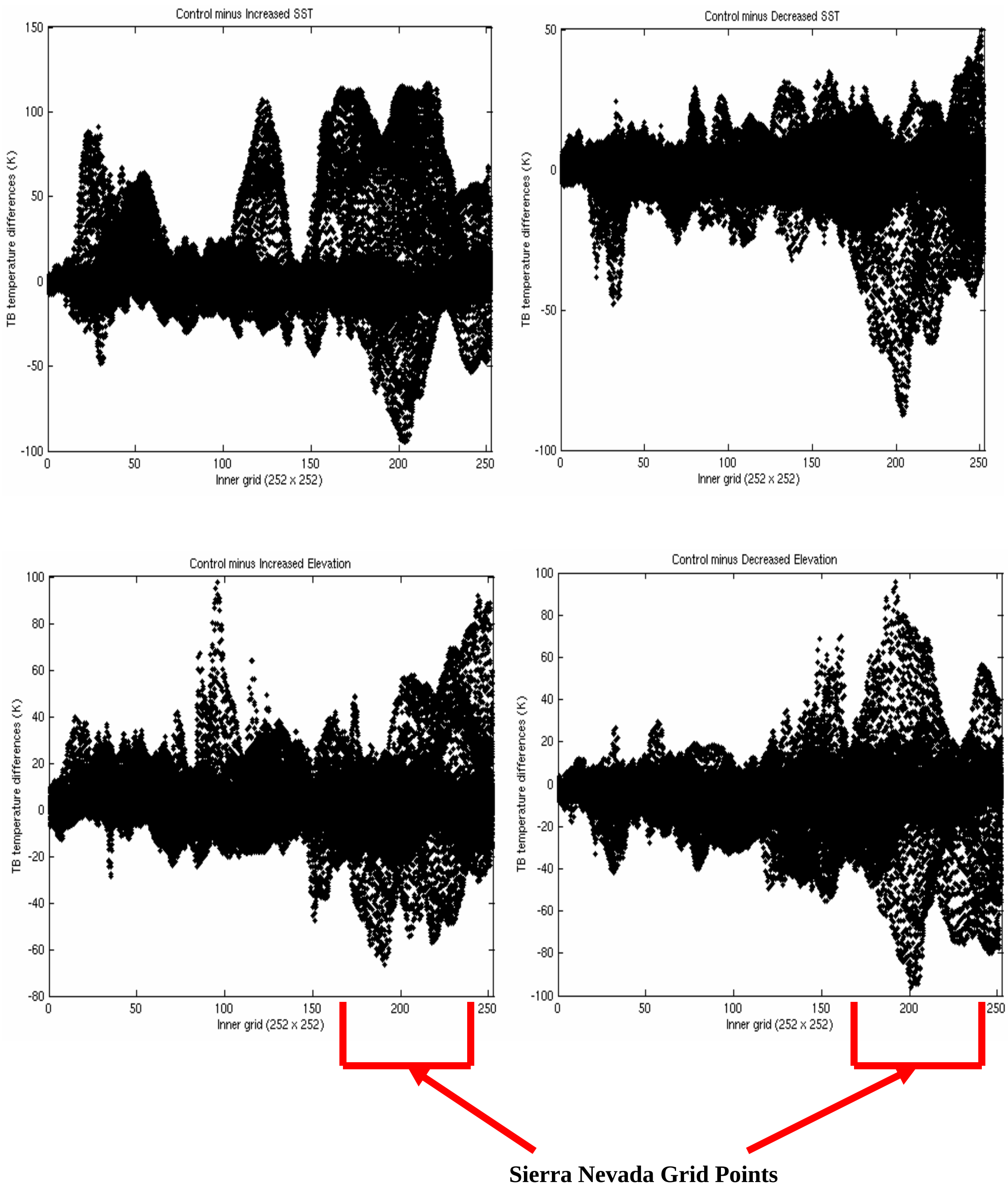

Control minus Increased SST
Control minus Decreased SST
Control minus Increased Elevation
Control minus Decreased Elevation
TB temperature differences (K)
Inner grid (252 x 252)
Sierra Nevada Grid Points

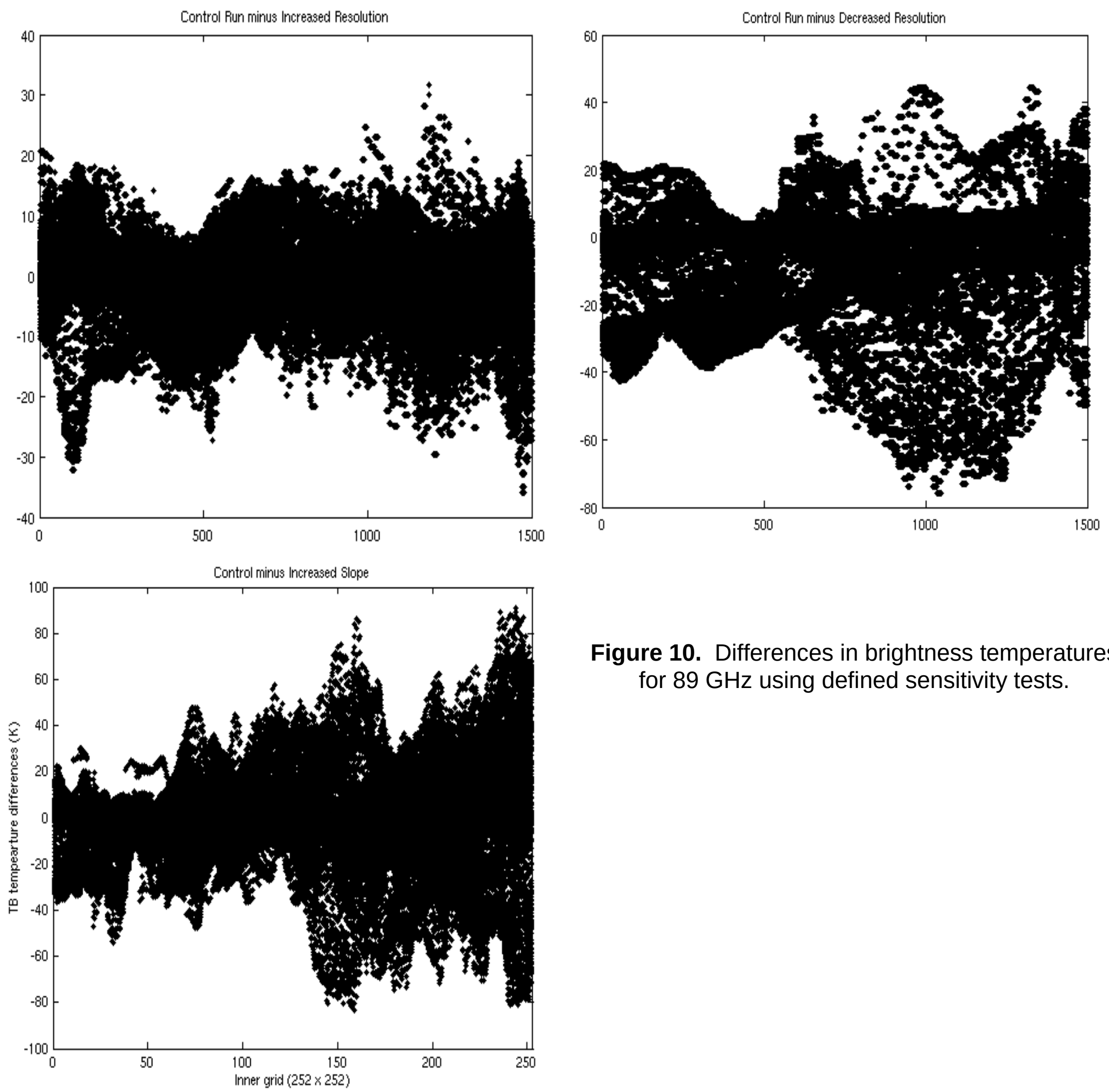

Figure 10. Differences in brightness temperatures for 89 GHz using defined sensitivity tests.

The biggest changes in 89.0 GHz brightness temperatures result from an increase in sea surface temperature and topography slope. Larger SSTs most likely enhance the amount of moisture available, increasing brightness temperatures for this channel. The steeper slopes throughout the domain most likely increase the degree of upslope flow occurring. Brightness temperatures fluctuate for reduced resolution because the ability to accurately resolve small scale precipitation clouds is lost. Luckily, increasing the resolution has the least impact on 89.0 GHz channels. Changing the height of the topography does not have as big of an impact as other variable changes, except over the

Sierra Nevada mountain points, where air parcels are forced to rise higher and condense more of their moisture. The 2 km inner domain size seems to be adequate for radiative transfer simulations. Since all of these variables produce significant brightness temperature changes, these chosen variables must be accounted for in the CDRD system.

This chapter has shown the capabilities of the UW-NMS in simulating orographic precipitation, along with possible tags that should be considered for the CDRD due to their accompanying TB sensitivities. The orographic precipitation event was analyzed for three different atmospheric levels. The jet stream, 700mb potential vorticity, surface moisture and 1-km winds are all important during this event. The following chapters discuss how the CDRD system is mined for the correct microphysical profiles, using the concept of data mining.

CHAPTER 7: CDRD DATA MINING

Precipitation retrieval involves sorting through huge amounts of data to obtain appropriate estimates of microphysical quantities. Sorting algorithms have typically been fairly slow. The CDRD retrieval scheme is based on the concept of data mining. Data mining is defined as the extraction of implicit, previously unknown, and potentially useful information from data. Data mining algorithms can learn from the available information as time progresses. Precipitation retrieval schemes based on data mining should continuously improve as the training algorithms improve their ability. Data mining is a unique tool that can significantly improve the effectiveness and efficiency of CDRD techniques because of the inherent learning ability and fast extraction of data.

Although relatively new to earth science, a few previous studies have made use of data mining schemes. Ramakrishnan (2004) used data mining algorithms to analyze large atmospheric aerosol datasets during the Exploratory Data Analysis and Management (EDAM) project. Ackerman (2004) used data mining procedures to study aerosol climate impacts and environmental interactions. This study was part of the Progressive Aerosol Retrieval and Assimilation Global Observing Network (PARAGON). Bankert (2004) applied data mining methods to numerical weather prediction (NWP) output and satellite data to develop algorithms to diagnose cloud ceiling heights in regions where no local observations were available. Finally, Tadesse (2005) used data mining to determine relationships between droughts in Nebraska and multiple climatic and oceanic indices. These indices include the Southern Oscillation index (SOI), the multivariate ENSO index (MEI), the Pacific-North American index (PNA), the Pacific decadal oscillation (PDO), and the North Atlantic Oscillation (NAO). Data mining was used to determine timelagged relationships between droughts and these indices. In all of the mentioned studies, the corresponding data warehouses are mined to determine previously unknown relationships between several seemingly unrelated parameters. Commonly used data mining techniques are: artificial neural networks, decision trees, genetic algorithms, nearest neighbor methods, and rule induction schemes.

Neural networks are analytic techniques that are modeled after the cognitive process of learning and the neurological functions of the brain. This method is capable of predicting new observations from previous observations. The technique is able to "*learn*" from existing data already present in the data warehouse. Denby (1993) discusses how artificial neural networks are used in high-energy physics research.

A decision tree is a model that is both predictive and descriptive (Frank and Whitten 2005). It is called a decision tree because the results are presented in the form of a tree structure. The visual structure of a decision tree makes the tool easy to understand. Decision trees are most commonly used for classification by predicting what group a case belongs to. Decision trees can also be used for regression, predicting a specific value. The primary output from a decision tree algorithm is the tree itself. Decision trees are commonly used in business to make decisions, based on *if-then* relationships.

Genetic algorithms are similar to the process of natural selection. This method searches for the most optimal matches based on certain criteria or combinations. The desired quantity ("organism") is retrieved based on the most optimal set of criteria ("genes"). Genetic algorithms have been used in finance but are not very practical as a data analysis tool. This is due to the lack of statistical significance from the obtained solution.

The nearest neighbor method, or sometimes referred to as the k-Nearest neighbor method, refers to similar data points, within a data warehouse, that are “living” in each other’s neighborhood. The “k” refers to the number of “neighbors” being investigated to retrieve a certain quantity. For example, 6-nearest neighbor looks at six neighbors. This data mining tool is more of a search technique than a learning tool. This technique is often used with small subsets of data.

Finally, rule induction is a data mining technique that extracts statistically significant data using if-then rules. Cohen (1995) presents a fast effective example of a rule induction technique. This tool can be used to infer generalizations from the information in the data.

A rule induction scheme is the best option to effectively mine data from the CDRD. This is based on the statistical properties that can be produced from any given retrieval. The proposed data mining scheme allows for the selection of microphysical profiles from the database using dynamical and thermodynamical variables linked to microphysical profiles. The CDRD mining algorithm retrieves the appropriate profiles and computes the corresponding variance, throughout the entire vertical atmospheric column. The matching of microphysical profiles with dynamic tags will rely on a Bayesian selection approach.

The goal of any retrieval database is to match space-measured brightness temperatures to microphysical atmospheric profiles, which can be used to calculate precipitation rates. The following chapter is an example of how the CDRD can be utilized to retrieve the “best-possible” microphysical profile for a particular event. Of particular focus is the severe storm that impacted California from January 7th - 11th, 2005, previously analyzed in this paper. A smaller (8 global simulations, including the

California case study) CDRD system is used to highlight the benefits of the CDRD approach.

CHAPTER 8: CDRD RETRIEVAL APPLICATIONS

This chapter is presented in two sections. The first section focuses on using the CDRD approach for the retrieval of more accurate microphysical profiles. A simulated retrieval is used for the Sierra Nevada case study. By using a CDRD approach the vertical variance in the retrieved microphysical profile is reduced. The second section uses an actual AMSU overpass to predict the probability of snow over northeast Colorado. The selected overpass was taken from October 10th, 2005. By using a Bayesian based approach, along with the CDRD tags, it is shown that the probability of snow can be increased by adding CDRD tag information.

The selected retrieval time is January 8th, 2005 at 12Z, over the case study inner domain. At first, microphysical profiles are selected from the 8-run sample CDRD database, using only brightness temperatures at 89.0 GHz. The idealized simulated TB field, derived from the UW-NMS, is taken as “truth” for selection of microphysical profiles from the CDRD. The goal is to retrieve the best profile for the Sierra Nevada region, where the majority of orographic precipitation is occurring. A simulated overpass suggests microphysical profiles should be selected from a range of brightness temperatures from 180 - 240K. These are the brightness temperatures that are observed over the mountain range.

Using the CDRD with only brightness temperatures is similar to a CRD approach. Next, profiles are selected using brightness temperatures paired with certain dynamical and thermodynamical tags. First, microphysical profiles are selected using the brightness temperatures along with mean sea level pressure and surface temperature. Second, profiles are selected using 89.0 GHz brightness temperatures, mean sea level pressure, surface temperature, and topography elevation. Since the database being used only contains 8 separate model runs, over the entire globe, three dynamical tags along with brightness temperatures is enough to correctly identify the desired California profiles.

The following table shows the range for each tag used and the number of microphysical profiles that are retrieved.

Parameter	**Range**		**Number of Profiles**
89.0 GHz Temps (K)	*180 - 240*		*132474*
Mean Sea Level Pressure (hPA)	*1008 - 1014*		*6138*
Surface Temperature (K)	*262 - 282*		*4990*
Elevation (m)	*700 - 4000*		

Table 5. This table shows the range for the CDRD tags used and the number of profiles mined from the sample database.

Notice that the number of possible microphysical tags decreases around 91 percent by adding only two dynamical tags. The tags are taken from the outermost grid of the UW-NMS, which uses 50km grid spacing. A follow-up paper uses an operational model such as the GFS forecasting system to obtain the dynamical tags.

The hypothesis, for showing the advantages of the CDRD approach, is that the vertical variance of microphysical profiles decreases as the number of dynamical tags increases. Figure 11 shows the mean vertical profile of total condensate mixing ratio. The mean changes as the number of profiles decreases. Figure 12 shows the structure of the variance for the selected microphysical profiles. When using only 89.0 GHz brightness temperatures, there is a significant amount of variance in the retrieved microphysical profiles. When dynamical tags are included, the variance of the retrieved profiles drops significantly, as shown in figure 12. This implies that the probability that the CDRD is producing a more accurate profile compared to the CRD approach is higher. When using the CDRD system for real-time applications it is theorized that more than two or three dynamical/ thermodynamical tags are needed to narrow the search for the “true” microphysical profile. In this case, the addition of the first two tags narrowed the focus to the California region. Eventually, the CDRD will be made up of hundreds of simulations globally.

This sample application of the CDRD system shows how the inclusion of large-scale dynamical tags can potentially be used to focus retrieval on more accurate profiles, thus improving estimation of precipitation rates from microwave based platforms.

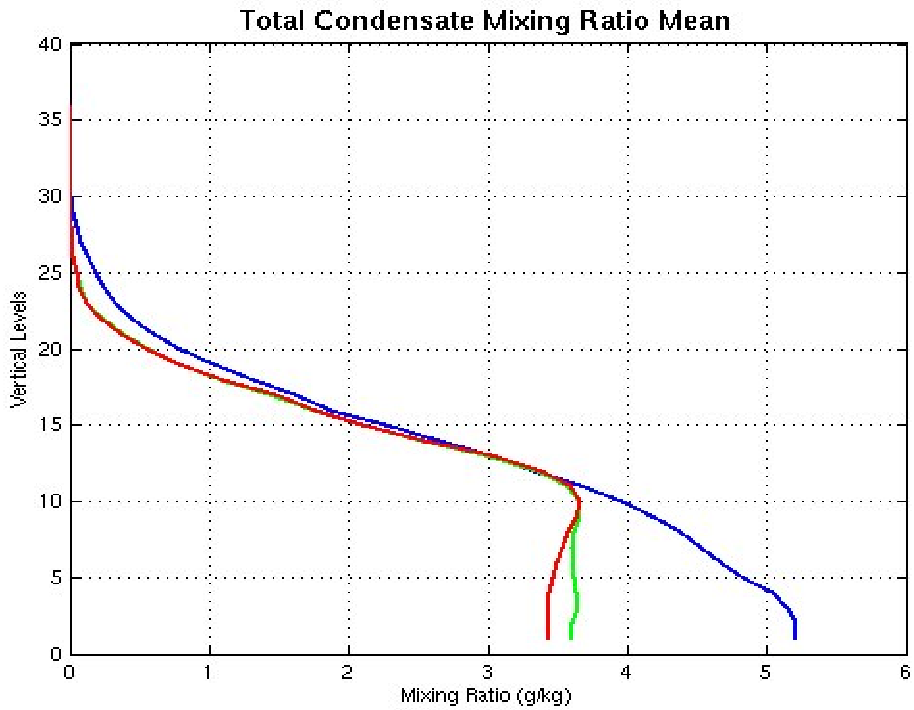

Figure 11. Vertically averaged total condensate mixing ratio mean. The average profiles were computed from using the CDRD tags shown below to extract the individual profiles.

Blue – 89.0 GHz

Green – 89.0 GHz, Mean Sea Level Pressure, and Surface Temperature

Red - 89.0 GHz, Mean Sea Level Pressure, Surface Temperature, and Elevation

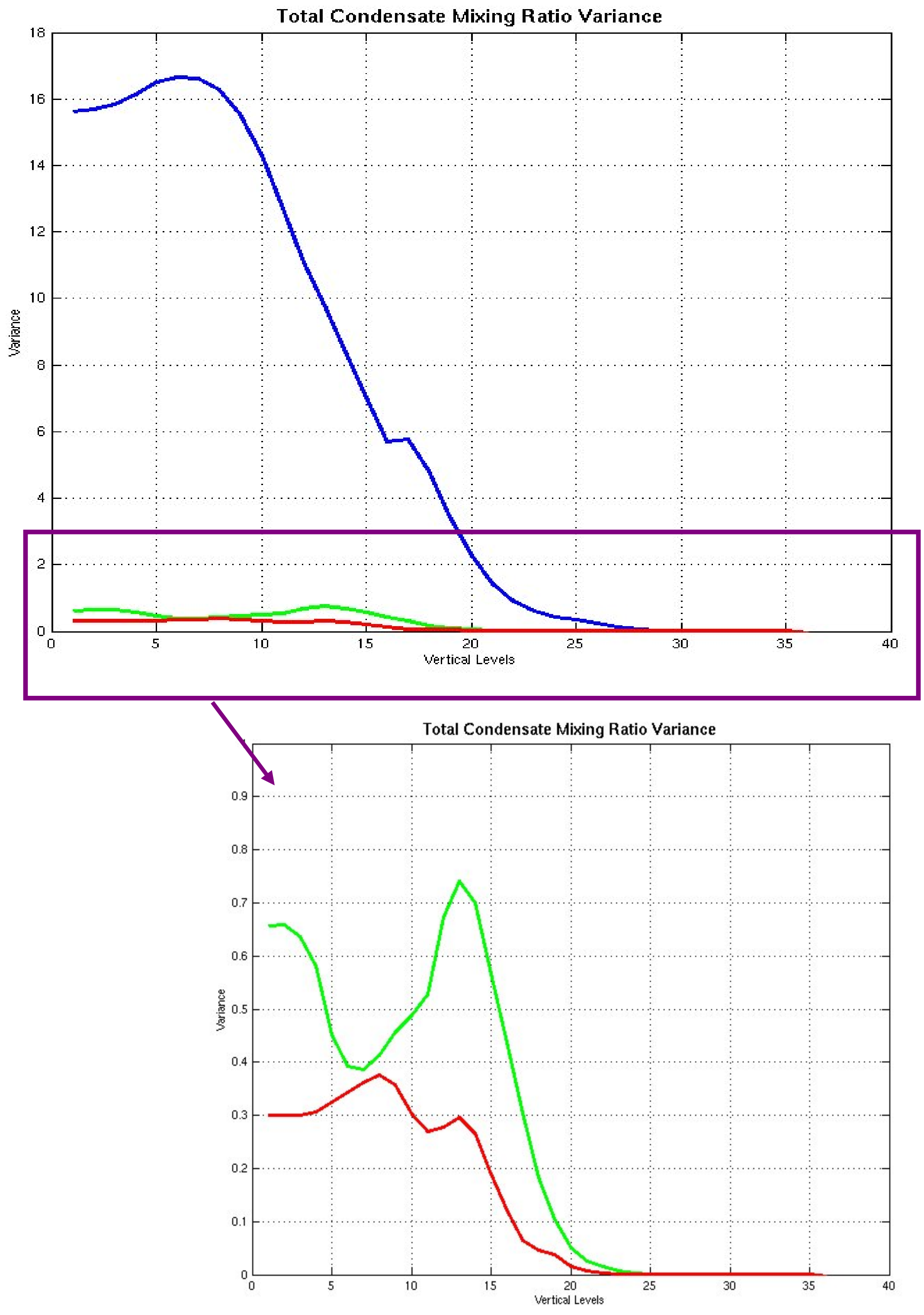

Figure 12. Vertically averaged total condensate mixing ratio variance. The variance profiles were computed using the CDRD tags shown below to extract the individual profiles.
Blue – 89.0 GHz
Green – 89.0 GHz, Mean Sea Level Pressure, and Surface Temperature
Red - 89.0 GHz, Mean Sea Level Pressure, Surface Temperature, and Elevation

Currently over 800,000 data measurement points are contained within the global CDRD, along with over 130 different model simulations. The following figure shows the current locations of the UW-NMS simulated inner grids.

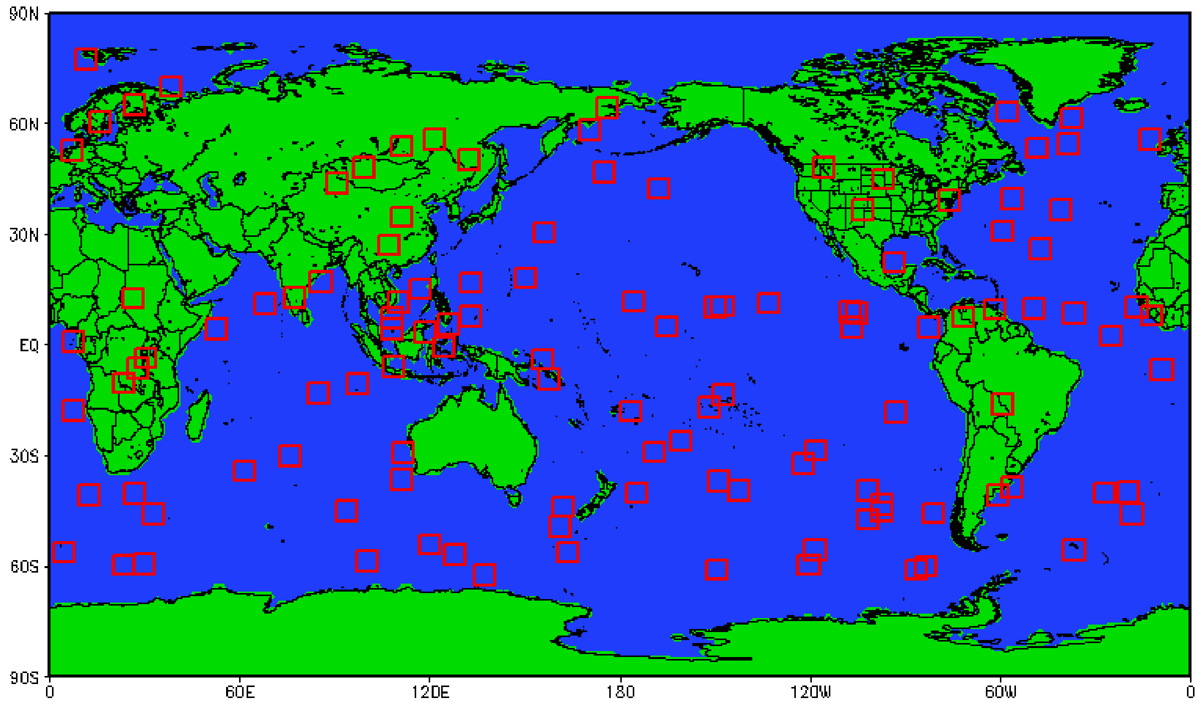

Figure 13. Current CDRD simulation locations as of February 10th, 2006.

` The final section of this thesis uses a Bayesian framework for showing the advantage of forecasting the probability of snowfall using CDRD tags. An early season snowstorm was impacting Northeastern Colorado on October 10th, 2005. The following images show the AMSU overpass and accompanying radar image around 1600Z.

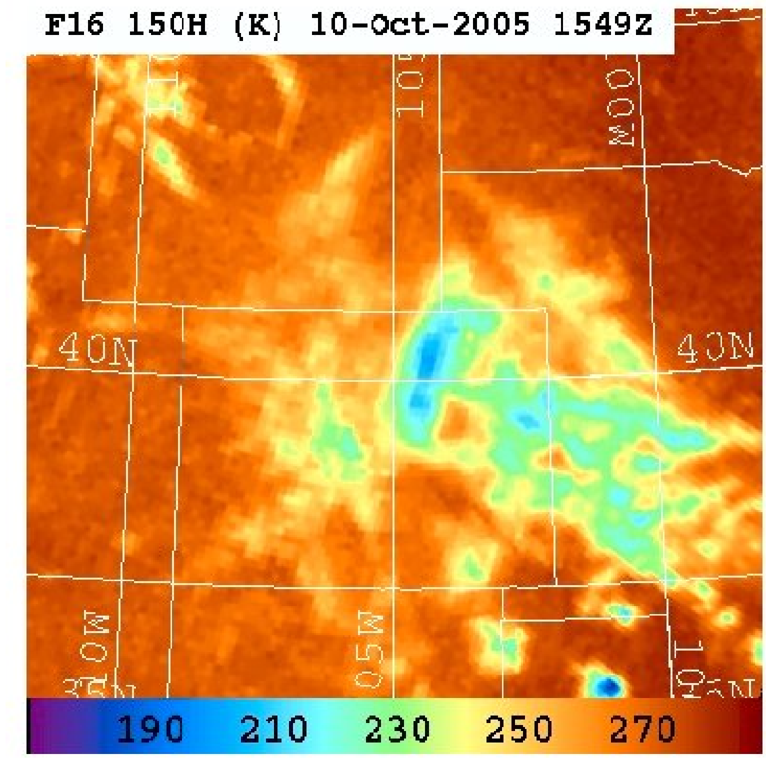

Figure 14. AMSU overpass for October 10th, 2005 at 1549Z at 150 GHz.

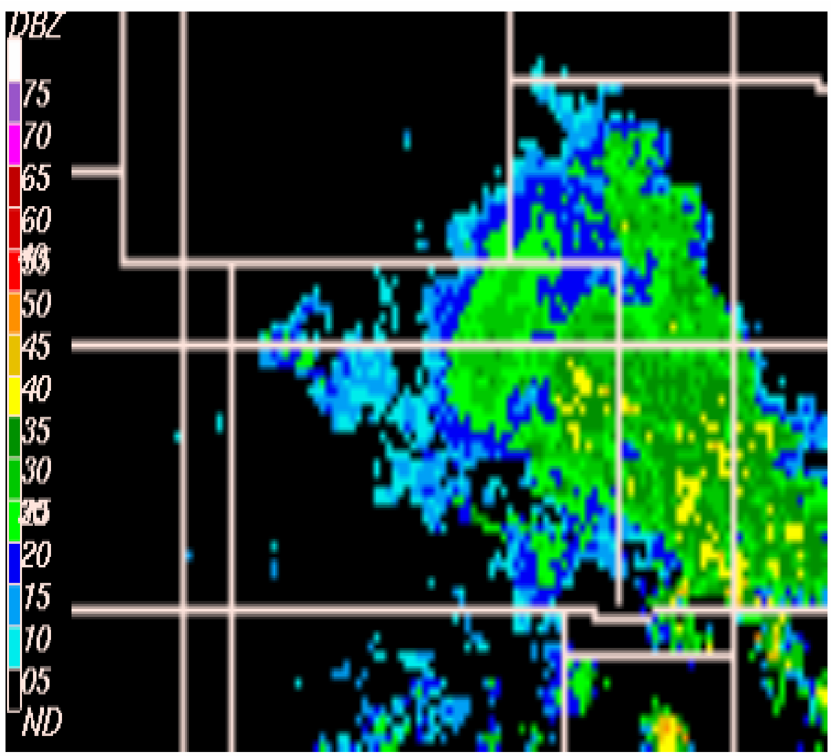

Figure 15. Radar reflectivity for October 10th, 2005 at 1549Z

The main goal of this section is to use the CDRD to determine the probability of a snowfall rate greater than 1mm/hr. Brightness temperatures are from the 150GHz AMSU channel. The temperatures range from 215 – 230K over the regions where snow is definitely falling, as indicated by the radar image. The probability of snow is first calculated using only brightness temperatures, similar to a CRD approach. The following Bayes' equation is used to calculate snow probability.

$$P(A \mid B) = \frac{P(A)P(B \mid A)}{P(B)}$$

A – Snowfall Rate > 1mm/hr
B – 150 GHz Brightness Temperatures from 215 – 230 K

Equation 6. Bayes' equation used for 1 variable.

P(A)	=	0.3893
P(B)	=	0.0724
P(B|A)	=	0.0920
P(A|B)	**=**	**0.4947**

Using only brightness temperatures gives a 49.47% chance of snowfall rate greater than 1mm/hr over the selected location. This is a concrete example of how similar brightness temperatures can occur with differing atmospheric conditions. If this brightness temperature range always corresponded with snow, the resulting Bayesian probability would be 100%. This highlights the need for a CDRD approach.

Next, Bayes' theorem is applied to a two variable approach. This is a simple example of the CDRD approach. The selected variable is surface temperature with a range of 271 – 277 K for the selected precipitation region. A GFS analysis is used to diagnose a range for surface temperature during the event. The following figure shows the surface temperature field.

Surface Temperature 10-OCT 2005 GFS ANALYSIS

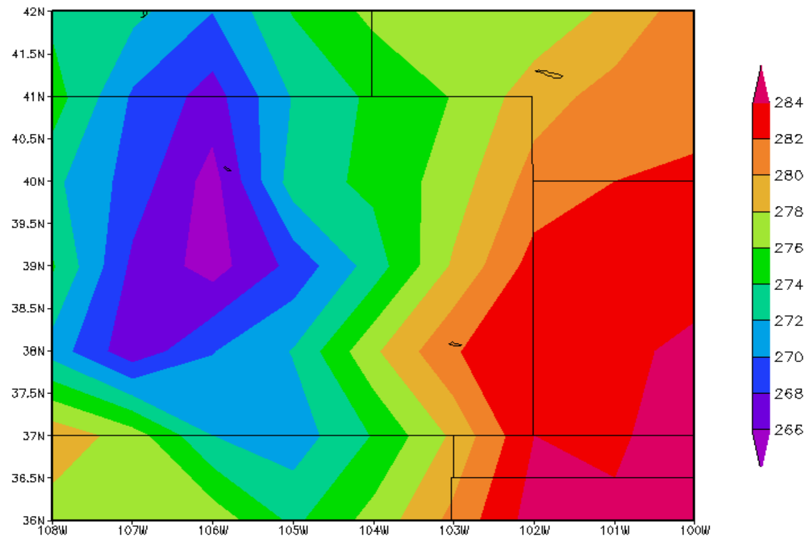

Figure 16. GFS Surface Temperature Analysis

The following Bayes' equation is applied to this case.

$$P(A \mid B, C) = \frac{P(A)P(B \mid A)P(C \mid A, B)}{P(B)P(C \mid B)}$$

Equation 7. Bayes' equation used for 2 variables.

A – Snowfall Rate > 1mm/hr
B – 150 GHz Brightness Temperatures from 215 – 230 K
C – Surface Temperature from 271 – 274 K

P(A) = 0.3893	
P(B) = 0.0724	P(C|A,B) = 0.2526
P(B|A) = 0.0920	P(C|B) = 0.1878
P(A|B) = 0.4947	**P(A|B,C) = 0.6655**

As is shown above, when using one dynamic variable, surface temperature, along with brightness temperatures, the probability of snowfall rates greater than 1mm/hr increases from 49.47% to 66.55%. The probability should be closer to 100% since snow rates greater than 1mm/hr are definitely occurring during the time period. The addition of one CDRD variable, which increases the probability of snow over the region, shows the usefulness of the approach.

Finally, Bayes' theorem is applied to a three variable approach. The second CDRD variable used is lifted index (LI). This variable represents the stability over the region, where higher values represent more stable regions. The sample measurement of LI is taken from a GFS analysis field. The following figure shows the lifted index with values ranging from 1-8 over the precipitation region.

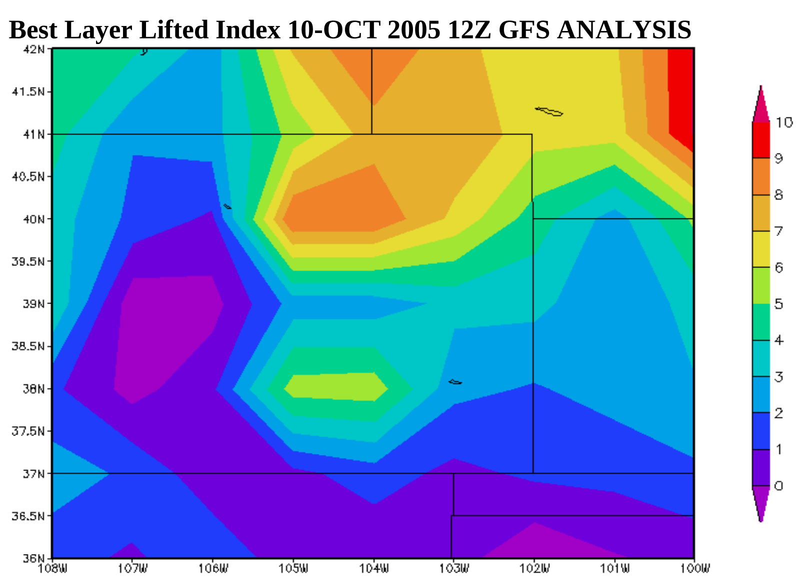

Figure 17. GFS Lifted Index Analysis

The following Bayes' equation is applied to this case.

$$P(A \mid B,C,D) = \frac{P(A)P(B \mid A)P(C \mid A,B)P(D \mid A,B,C)}{P(B)P(C \mid B)P(D \mid B,C)}$$

Equation 8. Bayes' equation used for 3 variables.

A – Snowfall Rate > 1mm/hr
B – 150 GHz Brightness Temperatures from 215 – 230 K
C – Surface Temperature from 271 – 274 K
D – Lifted Index from 1 - 8

P(A) = 0.3893		
P(B) = 0.0724	P(C|A,B) = 0.2526	P(D|A,B,C) = 0.7543
P(B|A) = 0.0920	P(C|B) = 0.1878	P(D|B,C) = 0.6028
P(A|B) = 0.4947	**P(A|B,C) = 0.6655**	**P(A|B,C,D) = 0.8327**

The addition of two variables really illustrates the advantage of using a CDRD approach compared to the current CRD approach. After using two dynamic variables the probability of snowfall rates greater than 1mm/hr increases to 83.27%. By using a CDRD approach the level of certainty for snowfall has increased by almost 35%.

CHAPTER 9: CONCLUSIONS

In recent years the accuracy of passive microwave remote sensing has been improving, with platforms such as SSM/I, AMSR, and TMI. Along with these new and improving satellites, precipitation retrieval algorithms have also been evolving. These algorithms rely heavily on cloud radiation databases (CRDs) to relate in-situ measurements of brightness temperatures to a-priori microphysical profiles found in CRDs. The CRD technique has worked relatively well in the past, yet there is still potential for improvement. Retrieved microphysical profiles are potentially mixed from differing atmospheric environments, such as stratiform and convective, or tropical and sub-tropical, etc. This can create inaccurate estimations of microphysical quantities and therefore inaccurate rainfall estimations. A new technique is proposed, the Cloud Dynamics and Radiation Database (CDRD), to improve these rainfall estimation uncertainties.

The CDRD system builds on the CRD concept, while including additional atmospheric information. Microphysical profiles are not only linked to brightness temperatures, but also a set of predefined dynamical and thermodynamical tags. These tags, along with other variables in the CDRD, are calculated from the University of Wisconsin Non-Hydrostatic Modeling System (UW-NMS). These tags are taken at a large-scale resolution, 50km, and a high-resolution, 2km. By adding additional variables to the current CRD approach, more accurate microphysical profiles are retrieved. The accuracy is improved by increasing the number of constraints for a Bayesian based retrieval approach.

The period from January 7th – 11th, 2005 brought extremely heavy rain to the California region. The majority of precipitation was influenced by topography i.e., the Sierra Nevada mountain chain. Orographic precipitation is a challenging quantity to retrieve accurately using passive microwave remote sensing techniques. A detailed case study of this event is presented, and the accuracy of the UW-NMS is documented by comparing rainfall accumulations during an orographically enhanced storm. Also, the SOI radiative model is used to calculate several different frequency brightness temperatures for the event.

This study shows that slight changes in certain parameters can alter modeled brightness temperatures by statistically large amounts. Four parameters in question, topography elevation, sea surface temperature, topography slope, and model resolution can thus play an important role in accurately determining brightness temperatures. Slight changes in any of these parameters change modeled brightness temperatures by statistically significant amounts. Brightness temperatures changed by over 100K in some sensitivity experiments.

Several data mining techniques and applications were discussed. A rule induction scheme best matches the technique used for retrieving information from the CDRD data warehouse. A sample CDRD database, 8 simulations, is used to highlight the benefit of using the CDRD approach, rather than a traditional CRD approach. The orographic case study over California is used to show the value added by using dynamic and thermodynamical tags, along with brightness temperature fields. By using these tags, the average vertical variance structure, in the profiles retrieved, significantly decreases. A more representative average microphysical profile is acquired. By using the CDRD tag approach, more accurate microphysical profiles can be retrieved from the accompanying database.

A snowfall case study was also presented to show the advantage of using a CDRD retrieval approach. An AMSU overpass captures an early season snowstorm over northeastern Colorado. When using a traditional CRD approach the probability of forecasted snow rates greater than 1mm/hr was only 49%. When employing a Bayesian based 2-variable CDRD approach the probability increases to 83%.

The CDRD is a robust system that has been shown to improve microwave precipitation retrieval techniques. This system can also be used for many other earth science applications. The CDRD is available online (http://cup.aos.wisc.edu/CDRD) and can be used to investigate many possible relationships between microphysical quantities and atmospheric parameters.

a. Future Work

The original idea for the CDRD concept is based on improving precipitation future retrieval algorithms. The CDRD is meant to improve retrieval algorithms before the launch of the Global Precipitation Measurement mission (GPM). Future CDRD work involves creating precipitation retrieval algorithms, such as GPROF, to work with a CDRD interface. These retrieval schemes will be based on a Bayesian approach. Work will continue on development of these algorithms.

The CDRD also provides many opportunities for other areas of atmospheric research. There has been interest in using the CDRD for lightning research, climate studies, and Antarctic precipitation studies. These research areas will be pursued as the size of the CDRD warehouse increases.

REFERENCES

Ackerman, T. P., A. J. Braverman, D. J. Diner, T. L. Anderson, R. A. Kahn, J. V. Martonchik, J. E. Penner, P. J. Rasch, B. A. Wielicki, and B. Yu. 2004: Integrating and Interpreting Aerosol Observations and Models within the PARAGON Framework. *Bulletin of the American Meteorological Society*: **85**, No. 10, 1523–1533.

Bankert, R. L., M. Hadjimichael, A. P. Kuciauskas, W. T. Thompson, and K. Richardson. 2004: Remote Cloud Ceiling Assessment Using Data-Mining Methods. *J. Appl. Meteorol.*, **43**, No. 12, 1929–1946.

Bergeron, T., 1935: On the physics of clouds and precipitation. *Proc. Fifth Assembly*. Lisbon, Portugal, UGGI, 20.

Cohen W. W., 1995: Fast effective rule induction. In Machine Learning, *12th International Conference,* Morgan Kaufmann.

Colle B. A., 2004: Sensitivity of Orographic Precipitation to Changing Ambient Conditions and Terrain Geometries: An Idealized Modeling Perspective. *J. Atmos. Sci.*, **61**, 588–606.

Denby B., 1993: The Use of Neural Networks in High Energy Physics, *Neural Computation*, **5**, num.4, 505-549.

Dettinger M., K. Redmond, D. Cayan, 2004: Winter Orographic Precipitation Ratios in the Sierra Nevada – Large-Scale Atmospheric Circulations and Hydrologic Consequences, *J. Hydrometeor*., **5**,1102-1116.

Ferriday, J. G., and S. K. Avery. 1994: Passive Microwave Remote Sensing of Rainfall with SSM/I: Algorithm Development and Implementation. *J. Appl. Meteorol.*, **33**, No. 12, 1587–1596.

Frank, E., I. H. Whitten, 2005: Data Mining: Practical Machine Learning Tools & Techniques with Java implementations, **2nd ed**., Morgan Kaufmann.

Galewsky J., A. Sobel, 2005: Moist Dynamics and Orographic Precipitation in Northern and Central California during the New Year's Flood of 1997, *Mon. Wea. Rev*., **6**, 1594-1612.

Heidinger A. K., C. O'Dell, R. Bennartz, T. Greenwald, 2005: The Successive Order of Interaction Radiative Transfer Model, Part I: Model Development, *J. Atmos. Sci*., submitted.

Houze, R. A. Jr., 1993. Orographic Clouds, in *Cloud Dynamics,* Academic Press, 502-538.

Kummerow C., L. Giglio, 1994: A Passive Microwave Technique for Estimating Rainfall and Vertical Structure Information from Space. Part II: Applications to SSM/I Data, *J. Appl. Meteor*., **33**, 19-34.

——, W. Barnes, T. Kozu, J. Shiue, and J. Simpson. 1998: The Tropical Rainfall Measuring Mission (TRMM) Sensor Package. *J. Atmos. Ocean. Tech.*, **15**, No. 3, 809–817.

——, Y. Hong, W. S. Olson, S. Yang, R. F. Adler, J. McCollum, R. Ferraro, G. Petty, D.-B. Shin, and T. T. Wilheit. 2001: The Evolution of the Goddard Profiling Algorithm (GPROF) for Rainfall Estimation from Passive Microwave Sensors. *J. Appl. Meteorol.,* **40**, No. 11, 1801–1820.

Lin, Y., S. Chiao, M. L. Kaplan.2004: Numerical Study of the Orographic Forcing of Heavy Precipitation during MAP IOP-2B. *Mon. Wea. Rev*., **132**, No. 9, 2184–2203.

Liou, K., and A. D. Duff. 1979: Atmospheric Liquid Water Content Derived from Parameterization of Nimbus 6 Scanning Microwave Spectrometer Data. *J. Appl. Meteorol.,* **18**, No. 1, 99–103.

Marwitz J. D., 1987: Deep Orographic Storms over the Sierra Nevada. Part II: The Precipitation Processes, *J. Atmos. Sci*., **44**, 174-185.

McCollum, J. R., and R. R. Ferraro. 2005: Microwave Rainfall Estimation over Coasts. *J. Atmos. Ocean. Tech.,* **22**, No. 5, 497–512.

Neiman, P. J., F. M. Ralph, A. B. White, D. E. Kingsmill, and P. O. G. Persson. 2002: The Statistical Relationship between Upslope Flow and Rainfall in California's Coastal Mountains: Observations during CALJET. *Mon. Wea. Rev*., **130**, No. 6, 1468–1492.

Petty, G. W., and K. B. Katsaros. 1990: Precipitation Observed over the South China Sea by the Nimbus-7 Scanning Multichannel Microwave Radiometer during Winter MONEX. *J. Appl. Meteorol.,* **29**, No. 4, 273–287.

——, and K. B. Katsaros. 1992: *Nimbus-7* SMMR Precipitation Observations Calibrated against Surface Radar during TAMEX. *J. Appl. Meteorol.,* **31**, No. 6, 489–505.

Prabhakara, C., D. A. Short, W. Wiscombe, R. S. Fraser, and B. E. Vollmer. 1986: Rainfall over Oceans Inferred from Nimbus 7 SMMR: Application to 1982–83 El Niño. *J. Appl. Meteorol.,* **25**, No. 10, 1464–1474.

Ramakrishnan, R., Schauer J.J., Chen, L., Gross, D.S., Huang, Z., Musicant D.R., and Shafer, M.M., The EDAM Project: Mining Atmospheric Aerosol Datasets, *J. Intel. Inf. Sys., Special Issue on KDD, 2004.*

Reynolds D. W., A. P. Kuciauskas, 1988: Remote and In Situ Observations of Sierra Nevada Winter Mountain Clouds: Relationships between Mesoscale Structure, Precipitation and Liquid Water, *J. Appl. Meteor*., **27**, 140-156.

Shafer, J. C., B. A. Colle, J. B. Wolfe, W. J. Steenburgh, D. E. Kingsmill, and J. A. W. Cox 2005: High-Resolution Simulations and Microphysical Validation of an Orographic Precipitation Event over the Wasatch Mountains during IPEX IOP3. *Mon. Wea. Rev*., **133**, No. 10, 2947–2971.

Shi, L., and J.J. Bates, 2005: Distribution and variability of atmospheric temperature and water vapor derived from HIRS measurement. *85th AMS annual meeting, San Diego, CA, 9-13 January 2005, combined preprints* CD-ROM, American Meteorological Society, Boston, MA, J6.1 (6 p.)

Smith E. A., J. E. Lamm, R. Adler, J. Alishouse, K. Aonashi, E. Barrett, P. Bauer, W. Berg, A. Chang, R. Ferraro, J. Ferriday, S. Goodman, N. Grody, C. Kidd, D. Kniveton, C. Kummerow, G. Liu, F. Marzano, A. Mugnai, W. Olson, G. Petty, A. Shibata, R. Spencer, F. Wentz, T. Wilheit, and E. Zipser. 1998: Results of WetNet PIP-2 Project. *J. Atmos. Sci.,* **55**, No. 9, 1483–1536.

Spencer, R. W., M. R. Howland, and D. A. Santek. 1987: Severe Storm Identification with Satellite Microwave Radiometry: An Initial Investigation with Nimbus-7 SMMR Data. *J. Appl. Meteor*., **26**, No. 6, 749–754.

Tadesse, T., D. A. Wilhite, M. J. Hayes, S. K. Harms, and S. Goddard. 2005: Discovering Associations between Climatic and Oceanic Parameters to Monitor Drought in Nebraska Using Data-Mining Techniques. *J. Climate*, **18**, No. 10, 1541–1550.

Tripoli G. J., 1992: A Nonhydrostatic Mesoscale Model Designed to Simulate Scale Interaction, *Mon. Wea. Rev*., **120**, 1342-1359.

Wilheit, T. T., J. S. Theon, W. E. Shenk, L. J. Allison, and E. B. Rodgers. 1976: Meteorological Interpretations of the Images from the Nimbus 5 Electrically Scanned Microwave Radiometer. *J. Appl. Meteor*., **15**, No. 2, 166–172.

——, C. D. Kummerow, and R. Ferraro, “Rainfall algorithms for AMSR-E,” *IEEE Trans. Geosci. Remote Sensing*, vol. 41, pp. 204–214, Feb. 2003.

Wilke, G. D., and M. J. McFarland. 1986: Correlations between Nimbus-7 Scanning Multichannel Microwave Radiometer Data and an Antecedent Precipitation Index. *J. Appl. Meteor*., **25**, No. 2, 227–238.